Anisotropic three-dimensional XY model and vortex-loop scaling

Subodh R. Shenoy and Biplab Chattopadhyay
School of Physics, University of Hyderabad, Hyderabad 500 134, Andhra Pradesh, India
(Received 29 December 1993)

Scaling equations are obtained for thermally excited vortex loops in the anisotropic three-dimensional (3D) XY model with interplane/intraplane coupling ratio $K_\perp/K_\parallel=\gamma_0^{-2}$. For high-$T_c$ superconductors, γ_0^{-2}, related to the Ginzburg-Landau masses, is in a strong anisotropy regime, $\gamma_0^{-1}<0.5$, and a length scale $r_0=\gamma_0 a_0$ naturally arises ($a_0=$ lattice constant). (i) For loop major axes $a>r_0$, the dominant excitations are 3D elliptical vortex loops cutting multiple planes, with $a\sim\xi_-(T)=a_0|\varepsilon|^{-\nu}$ where $|\varepsilon|\equiv|(T-T_c)/T_c|$, and $\nu=0.67$. The vorticity segment components ($\mu=\hat{x},\hat{y},\hat{z}$) are $J_\mu(r)=0,\pm1$, and interact via a Biot-Savart-like law. The renormalized anisotropy $\gamma_l^{-1}\to1$, asymptotically isotropic, as $l=\ln(a/a_0)\to\infty$: anisotropy is irrelevant. (ii) For loop scales $r_0>a>2a_0$ the dominant excitations are quasi-2D rectangular loops with short sides $J_z(r)=\pm1$ cutting single planes, that are thus effectively decoupled at *finite* scales $<r_0$. The $J_z=\pm1$ vortex components, of in-plane separation $|\vec{R}_\parallel|<r_0$, interact via a logarithmic $[\ln(|\vec{R}_\parallel|/r_0)]$ plus linear $[Q_0(|\vec{R}_\parallel|/a_0-1)]$ potential. As $\gamma_0^{-1}\to0$, the coefficient $Q_0\to0$, and the Kosterlitz-Thouless limit is recovered. (iii) The 3D transition temperature T_c versus $K_\perp/K_\parallel$, calculated for strong anisotropies from "2D" (3D) scaling for scales $<r_0$ ($>r_0$), matches existing Monte Carlo data well. Critical regions $|\varepsilon_c|\le\gamma_0^{-1/\nu}$ are estimated. Contact is made with ideas of an intrinsic critical current arising from linear $\sim\gamma_0^{-1}R_\parallel$ vortex segment effective potentials.

I. INTRODUCTION

High-T_c superconductors[1] (HTS's) have been subject of intense research, since their discovery in 1987. Whatever the underlying mechanism, the new layered materials share with the ordinary superconductors the property of a macroscopic *scalar phase* $-\pi<\theta\le\pi$, whose gradient is the superfluid velocity. Josephson junctions between the old and new superconductors support a tunneling supercurrent;[2] segmented rings of the two materials carry a persistent supercurrent;[3] and flux quantization, originating from multivaluedness of the (gauge-invariant) phase has been observed.[4] Thus lattice models of coupled planar "XY" spins $-\pi<\theta_i\le\pi$, or phases in a layered 3D structure, are relevant to HTS's.

In fact, signatures of topological (vortex) phase excitations have also been reported in the layered HTS's (Ref. 5) and their artificial superlattices (Ref. 6). The nonlinear I-V characteristics and resistances show[5] signatures of the two-dimensional (2D) vortex unbinding or Berezinskii, Kosterlitz-Thouless (KT) transition[7] such as occurs in strictly 2D Josephson-junction arrays[8] (JJA's) and 2D planar or XY ferromagnets.[9] (An effective decoupling of layers above T_c has been suggested[10] to account for this.) Vortex-point 2D scaling methods, developed for the 2D XY model,[9] have been applied[11] to (3D) high-T_c materials.

On the other hand, there is increasing evidence that the high T_c superconductors fall into the 3D XY universality class.[12] Three-dimensional vortex-loop excitations have been invoked to understand HTS transition temperatures.[13] The puzzle[14] of how 2D vortex behavior can be so prominent in phase-coherent HTS's, and yet coexist with 3D critical behavior, motivates a study of topological vortex excitations of the layered 3D XY model. Some microscopic models[15] for HTS's involve quantum capacitive Josephson arrays, in two dimensions, that are equivalent to (2+1)D classical XY models with an extra "time" dimension in a path integral formalism. Once again, this motivates a study of the anisotropic 3D XY model.

In this paper, we generalize a previous (isotropic) 3D vortex-loop scaling approach,[16,17] to the anisotropic 3D XY model. The dominant topological excitations at large and small scales are identified, and scaling equations for the fugacity and coupling are obtained. The transition temperature T_c is calculated, and the length scale $\xi_+(T)$ for $T>T_c$ is shown to have both quasi-2D (noncritical) and 3D (critical) temperature dependences. Critical regions are estimated.

The Hamiltonian is

$$H=-\sum_{\mu=\hat{x},\hat{y},\hat{z}}\sum_i \mathcal{J}_\mu[\cos(\Delta_\mu\theta_i)-1]\,, \tag{1.1}$$

where the phase variables $-\pi<\theta_i\le\pi$ are on layered lattice sites $\{i\}$, with nearest-neighbor coupling and lattice constant $\mathcal{J}_\parallel,a_\parallel$ ($\mathcal{J}_\perp,a_\perp$) within (between) planes as in Fig. 1. Δ_μ is a discrete derivative in the $\mu=\hat{x},\hat{y},\hat{z}$ directions. This can be transformed[18] to a model for directed vorticity loop segments $\mathcal{J}_\mu(r)=0,\pm1$, interacting via the Biot-Savart potential. Each closed loop is a toroidal spin-tilt configuration, and a tumbling loop corresponds to a stirring up of the phases, on a scale of the average loop diameter.

A physical realization of the model is a layered 3D JJA with superconducting grains at the lattice sites and different intergrain oxide thickness within and between planes, so the Josephson coupling ratio $\mathcal{J}_\perp/\mathcal{J}_\parallel\neq1$. Resistance and current-drive effects in 3D JJA, based on these

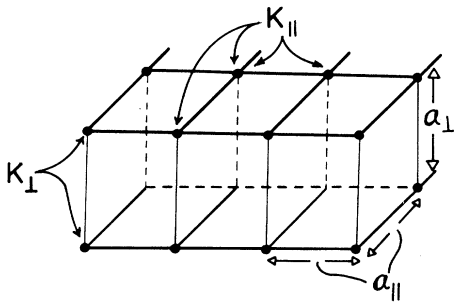

FIG. 1. Anisotropic layered 3D XY lattice couplings $K_\perp, K_\parallel$ and lattice parameters $a_\perp, a_\parallel$.

vortex-loop scaling results, will be presented elsewhere.[19] (Effects of weakly fluctuating gauge fields are not included at this stage, as the essential nature of the transition is unaffected[20,17(b)]).

Equation (1.1) can be regarded as a weakly ($\mathcal{J}_\perp$) coupled, layered, Ginzburg-Landau (GL) Lawrence-Doniach model,[21] with pair-wave function magnitudes $|\psi|$ locked and planes composed of $\mathcal{J}_\parallel$-coupled in-plane coherent regions $\sim a_0$. Magnitude fluctuations are ignored as $|\psi|^2 \propto (1-T/T_{\rm GL})$ and the phase locking temperature $T_c \ll T_{\rm GL}$ the magnitude locking temperature. Then $\gamma_0^{-2} \equiv (\mathcal{J}_\perp/\mathcal{J}_\parallel) = M_\parallel/M_\perp$ is the ratio of the Ginzburg-Landau masses. HTS's are in a "strong anisotropy regime," $\gamma_0^{-1} < 0.5$, with[11(f)] $\gamma_0^{-1} \sim 0.014$ (thallium) and $\gamma_0^{-1} \sim 0.2$ (yttrium).

Feynman and Onsager[22] had proposed a vortex-loop blowout picture of bulk superfluid-to-normal or λ transition. It was conjectured by Halperin[23] that vortex loops with a topological current $J_\mu(r) = 0, \pm 1$ (interacting via a Biot-Savart potential) could provide an alternative description of the 3D XY transition. The loops exist: they can be seen visually in simulations[24,25] blowing out at transition. Monte Carlo (MC) isotropic 3D XY simulations by Kohring, Shrock, and Wills showed[26] that suppressing vorticity by an external chemical potential suppressed the transition out of the ordered state. Thus, the vortex loops are involved in the transition. Williams[16] and Shenoy[17] proposed a vortex-loop scaling approach and used it to calculate (isotropic case) critical properties. Thus, the loops are spin-collective variables, sufficient to describe the transition. Recent MC work[24,25] on the anisotropic 3D XY model showed the transition temperature was pushed down as interplane coupling weakened, approaching the KT value, as $\mathcal{J}_\perp/\mathcal{J}_\parallel \to 0$. Thus, the 3D vortex loops must have configurations that go over to 2D vorticity ± 1 pairs, as planes decouple completely.

The physical picture[16,17] of the (isotropic XY), transition involves thermally activated vortex loops, which increase in number and average diameter $a = a_0 e^l$ on warming, where a_0 is the lattice constant. Nesting of smaller loops and consequent screening of large loops weakens their binding, allowing further expansion and nesting, until the largest loop $a \sim \xi_-(T) \sim (T_c - T)^{-\nu}$ blows out at $T = T_c$. The transverse direction fluctuations around the mean circle define a core size[17,27] a_c that also blows out, $a_c \propto a \sim \xi_- \to \infty$.

The results of the anisotropic generalization are as follows.

Excitations. The anisotropy ratio $\gamma_0^{-2} \equiv \mathcal{J}_\perp/\mathcal{J}_\parallel$ defines a regime of strong planar anisotropy ($\gamma_0^{-1} < 0.5$) and a length scale[28] in this regime, $r_0 = \gamma_0 a_0 > 2a_0$. For a characteristic loop length scale $a \equiv a_0 e^l$, defined as the loop extent in the x-y plane, there are three types of excitations, depending on the scale. For $a > r_0$, multiplane tumbling elliptical loops dominate, with loop fugacity $y_l(\alpha)$ dependent on loop orientation α with reference to the z axis. $y_l(\alpha)$ is peaked for (circular) loops parallel to the plane ($\alpha = \pi/2$), while ellipse eccentricity is maximum for $\alpha = 0$, loops perpendicular to planes. For $a < r_0$, ellipses are angularly constrained from tumbling freely and have orientation constrained to be around the plane, $\alpha \approx \pi/2$. Rectangular loops appear, of vertical unit sides of vorticity $J_\perp(\mathbf{r}), J_\perp(\mathbf{r}') = \pm 1$, and long sides of length $|\mathbf{r}_\parallel - \mathbf{r}'_\parallel| < r_0$. Since they cut only single planes independently, they have a quasi-2D character.

Interactions and scaling equations. The interaction $U(\mathbf{r}-\mathbf{r}')$ between vortex segments $\mathbf{J}(\mathbf{r}), \mathbf{J}(\mathbf{r}')$ is of the Biot-Savart type, $U(\mathbf{r}-\mathbf{r}') \sim |\mathbf{r}-\mathbf{r}|^{-1}$. For $\gamma_0^{-1} \to 0$, i.e., scales $a < r_0 \to \infty$, the potential $U(\mathbf{r}-\mathbf{r}') \sim \ln(\mathbf{r}_\parallel - \mathbf{r}'_\parallel)\delta_{z,z'}$ is logarithmic between $J_\perp(\mathbf{r}), J_\perp(\mathbf{r}) = \pm 1$, and confined to the decoupling planes. The 2D Kosterlitz-Thouless limit is thus recovered. For γ_0^{-1} small but nonzero, the $\mathbf{J}_\parallel$ sides of the single-plane or quasi-2D loops, contribute an effective linear potential $\sim Q_0(|\mathbf{r}_\parallel - \mathbf{r}'_\parallel|/a_0 - 1)$ between the $J_\perp = \pm 1$ unit sides. The coefficient $Q_0 \sim \gamma_0^{-2}$ (γ_0^{-1}) with (without) screening from the in-plane circular loops. This result makes contact with linear potentials (and consequent intrinsic in-plane critical currents) obtained from simulations, and variational estimates.[10(e)]

2D scaling equations for $a < r_0$ for the vortex coupling $K_l^{(2D)}$ and $J_\perp = \pm 1$ pair fugacity $y_l^{(2D)}$ are KT-like, with corrections from the linear potential. At $a = r_0$, they feed into 3D scaling equations for $a > r_0$ for K_l and (angularly averaged) y_l, couplings and loop fugacities, which are of the same form as the isotropic 3D case. The larger loops see an effective anisotropy γ_l^{-1} progressively smoothed over by the smaller tumbling loops, and γ_l^{-1} scales asymptotically to zero. The fixed points and critical exponents are thus unchanged: anisotropy is irrelevant.

Transition temperature. $T_c(\gamma_0)$ is determined by changes in the (3D) asymptotic scaling flows, as the temperature T is varied. $\bar{T}_c \equiv k_B T_c/\mathcal{J}_\parallel$ versus γ_0^{-2} matches the MC data reasonably well, including 3D isotropic ($\gamma_0^{-1} = 1$, $\bar{T}_c = 2.2$) and 2D ($\gamma_0^{-1} = 0$, $\bar{T}_c = 0.91$) limiting values.

Critical and noncritical temperature dependences. Above T_c, the separation $\xi_+(T)$ between (correlated) segments can be defined in terms of the single-segment vorticity density n_v at large scales, $\xi_+ \sim n_v^{-1/3}$, with $n_v = y_l^{1/2}/a^3$ as $a \to \infty$. $\xi_+(T)$ is found to have 3D critical[29] behavior $\sim |\epsilon|^{-\nu}$ ($\nu = 0.67$) as $|\epsilon| \equiv |(T - T_c)/T_c| \to 0$, and to have KT-like noncritical

behavior $\xi_+ \sim \exp\{[T/T_{KT}(\gamma_0)-1]^{-1/2}\}$. Here $T_{KT}(\gamma_0)$ is defined by a KT-like condition[9] for finite-scale unbinding of the quasi-2D excitations, $\pi K_{l_0}^{(2D)}(T_{KT}) \approx 2$, where $l_0 \equiv \ln(r_0/a_0)$. Critical ($|\epsilon_c|$) and crossover regions in $|\epsilon|$ can be estimated by 5% deviations from the 3D, "2D" limiting behaviors, with $\epsilon_c < \gamma_0^{-1/\nu}$.

The plan of the paper is as follows. In Sec. II we consider the vortex-loop Hamiltonian (derived from the cosine Hamiltonian in Appendix A) and its limiting cases. The bare orientation-dependent fugacity, $y_0(\alpha)$ is discussed, with details of derivation in Appendix B. In Sec. III the anisotropic elliptical loop scaling equations that control large scales $a > r_0$ are obtained, with details in Appendix C. Section IV presents modified quasi-2D scaling equations for finite scales $a < r_0$ (that feed into the asymptotic 3D equations) in the strongly anisotropic regime. The critical temperature $\bar{T}_c$ versus the anisotropy (γ_0^{-2}) curve is numerically found from asymptotic (3D) changes in scaling flows and compared with MC data. Critical regions are estimated. Section V is a summary and discussion of results.

II. VORTEX LOOPS IN THE ANISOTROPIC 3D XY MODEL

We first briefly summarize the vortex-loop approach[16,17] to the isotropic 3D XY model. The Hamiltonian of the planar spins on a cubic lattice $\{i\}$ of lattice constant $a_0=1$ is, as in (1.1), $\beta = 1/k_B T$,

$$\beta H = -\beta \mathcal{J} \sum_{\mu=\hat{x},\hat{y},\hat{z}} \sum_i \cos(\Delta_\mu \theta_i - 1) \ . \tag{2.1}$$

A standard dual transform[18(b)] maps this nearest-neighbor, angle variable $\{-\pi < \theta_i \le \pi\}$ model onto a directed vortex loop $\{\mathbf{J}_\mu(\mathbf{r})\}$ model, with long-range interactions:

$$\beta H \simeq \frac{\pi K_0}{2} \sum_{\mathbf{r}\neq\mathbf{r}'} \mathbf{J}(\mathbf{r})\cdot\mathbf{J}(\mathbf{r}')\tilde{U}(\mathbf{r}-\mathbf{r}') \ . \tag{2.2}$$

Here $J_\mu(\mathbf{r}) = 0, \pm 1, \ldots$ with directions $\mu = \hat{x},\hat{y},\hat{z}$ are integer-valued topological current components or 3D vortex variables, on the bonds of a cubic dual lattice of sites $\{r\}$. The bare vortex coupling is approximately related to the original cosine coupling $K_0 \simeq \beta\mathcal{J}$. The segments $\mathbf{J}$ form closed loops. $\tilde{U}(R)$ is the 3D lattice Green's function, with the $R=0$ part subtracted,

$$\begin{aligned}\tilde{U}(\mathbf{R}) &= [U(\mathbf{R}) - U(0)] \\ &= \int \frac{d^3q\, a_0^3}{(2\pi)^3} \\ &\quad \times \frac{4\pi(e^{i\mathbf{q}\cdot\mathbf{R}}-1)}{[6-2\cos q_x a_0 - 2\cos q_y a_0 - 2\cos q_z a_0]} \ ,\end{aligned} \tag{2.3}$$

where the integral is over the Brillouin zone.

A dual-lattice vortex loop corresponds to a quasi-toroidal original-lattice spin arrangement in the XY case or supercurrent flow in the superfluid helium case. This can be seen by a reverse dual transform[30] putting $\mathbf{J}(\mathbf{r}) \to \mathbf{J}(\mathbf{r}) + \mathbf{J}^{\text{ext}}(\mathbf{r})$, where $\mathbf{J}^{\text{ext}}(\mathbf{r})$ is externally fixed. One finds, by going back to $\{\theta_i\}$ variables, that they are[30] appropriately biased around the $\mathbf{J}^{\text{ext}}(\mathbf{r})$ line. Tumbling of loops is then a stirring of spins on the scale of the average loop diameter.

Identifying the $\mathbf{J}$ segments by the loops $\{L\}$ to which they belong, each loop is closed,

$$\Delta\cdot\mathbf{J}^{(L)}(\mathbf{r}) = 0 \forall L \ , \tag{2.4}$$

and the interaction energy can be separated into an inter-loop part ($L \neq L'$) and an intraloop part ($L = L'$). The partition function is then

$$Z = \sum_{\{\mathbf{J}^{(L)}(\mathbf{r})\}} \exp\left[-\frac{\pi K_0}{2} \sum_{L\neq L'} \sum_{\mathbf{r}\neq\mathbf{r}'} \mathbf{J}^{(L)}(\mathbf{r})\cdot\mathbf{J}^{(L')}(\mathbf{r}')U(\mathbf{r}-\mathbf{r}')\right] \prod_L y_0^{(L)} \tag{2.5}$$

where $U(R) \sim R^{-1}$ asymptotically. As discussed in Appendix A, the configuration sum is over values $J_\mu^{(L)} = \pm 1$ of the closed loops, and integral over their center of mass $\mathbf{R}^{(L)}$ and relative $\boldsymbol{\rho}^{(L)}$ coordinates, $\int d^3R^{(L)}/a_0^3 \int d^3\rho^{(L)}/a_0^3$. (For circular loops, $|\boldsymbol{\rho}^{(L)}| = \frac{1}{2}a_L$, with $\frac{1}{2}a_L$ being a fixed mean radius.) The constant part $U(0)$ in (2.3) is a segment self-energy, and by loop closure, $\sum_{\mathbf{r}} J_\mu^{(L)}(\mathbf{r}) = 0$, is absorbed into the fugacity $y_0^{(L)}$. The bare fugacity is

$$\begin{aligned} y_0^{(L)} &= \exp\left[-\frac{\pi K_0}{2} \sum_{\mathbf{r}\neq\mathbf{r}'} \mathbf{J}^{(L)}(\mathbf{r})\cdot\mathbf{J}^{(L)}(\mathbf{r}')U(\mathbf{r}-\mathbf{r}') - \frac{\pi}{2}K_0 U(0) \sum_{\mathbf{r}} [\mathbf{J}^{(L)}(\mathbf{r})]^2\right] \\ &\simeq \exp\left[-\pi^2 K_0 \frac{a_L}{a_0} \ln\frac{a_L}{a_c}\right] \ , \end{aligned} \tag{2.6}$$

where we have considered effectively circular loops of diameter a_L and absorbed $U(0)$ into the cutoff or core scale a_c. For $L=1$ minimum-size loops, $a_{L=1} = a_0$, and $y_0^{(L=1)} \equiv y_0$ is the smallest-loop bare fugacity with[17(a)] $y_0 = e^{-5.631K_0}$. At a general minimum scale $a = a_0 e^l$, the effective core size becomes scale dependent: $a_c = a_c(l)$. Loop segments can cross perpendicularly on the lattice without local energy cost. So, there are no permanent en-

tanglement effects. The scaling procedure integrates out smaller loops of all separations from the segment under consideration, including the loop touching the segment. Thus, we must exclude such "bubbles" to avoid double counting, and consider only quasicircular, crinkled, but self-avoiding loops, of all scales. It is this class of loops that can nest, screen, and blowout at transition.

The actual closed-loop configuration is as in Fig. 2,[27] with an average circular perimeter of diameter $a \equiv a_0 e^l$ and random transverse excursions, (like hairpins of a distorted U shape) within a core region of size $a_c(l)$. The interaction energy between the segments on loop L and a far off $L \neq L'$ segment $\mathbf{J}^{(L')}(\mathbf{r}')$ is $\sim \mathbf{J}^{(L')}(\mathbf{r}') \cdot (\sum_r \mathbf{J}^{(L)}(\mathbf{r})/|\mathbf{r}-\mathbf{r}'|)$. The magnetic field of a current-carrying electric wire is cut down drastically if the wire is folded back along itself in a narrow hairpin or U shape. Similarly the Biot-Savart-like potential at r' of a width W hairpin of the loop will be cut down by factors $\sim W/r' \ll 1$ through cancellation of contributions from oppositely directed hairpin sides. Only the azimuthal, uncanceled segments[27] of the hairpin will contribute appreciably to the large-distance potential. These uncancelled segments, scattered over the core region a_c, will add up vectorially in the azimuthal direction to an effective perimeter $\sim \pi a$. The complex topological current distribution, as far as the outside world is concerned, can thus be represented[27] as an effective circular loop of average diameter a, and core cutoff a_c, within which the irrelevant hairpin details are hidden. This is schematically depicted in Fig. 2.

The effective loop length πa_L depends on the actual perimeter p_L as $a \sim p_L^{\delta}$ with $\delta < 1$. A numerical simulation[27] suggests that $\delta \approx 0.4$. The intraloop interaction energy from the uncancelled azimuthal segments goes as $\sim a_L \ln a_L / a_c$, as stated above. The antiparallel sides of the hairpins contribute relatively little to the intraloop energy of large average diameter loops. For hairpins of width $W \ll a_L$, the antiparallel segments partially cancel the segment self-energy contributions at a general minimum diameter a, that scales all lengths. From $U(R)$ of (2.3) for antiparallel hairpin sides,

$$\sum_{\mathbf{r}(\neq \mathbf{s})} \mathbf{J}^{(L)}(\mathbf{r}) \cdot \mathbf{J}^{(L)}(\mathbf{s}) U(\mathbf{r}-\mathbf{s}) + \sum_{\mathbf{r}} [J^{(L)}(\mathbf{r})]^2 U(0)$$

$$\sim U(0) - U(W/a) \sim (W/a)^2 \ll 1 ,$$

which, moreover, scales to zero for a general scale $a \gg W$. Thus only (noncancelled) azimuthal segments are considered, in the segment self-energy and segment interaction, making up the loop self-energy. Both the interloop and intraloop energy contributions depend only on the diameter "a" and cutoff $a_c \propto a$, in an effective circular-loop picture.

Following the Kosterlitz[9] procedure, the scaling equations for the interloop coupling K_l and the loop fugacity y_l at a general minimum scale $a \equiv a_0 e^l$ are[16,17]

$$\frac{dK_l}{dl} = K_l - A_0 K_l^2 y_l , \tag{2.7a}$$

$$\frac{dy_l}{dl} = (6 - \pi^2 K_l L_l) y_l , \tag{2.7b}$$

where $A_0 \equiv 4\pi^3/3$, $L_l \equiv 1 + \ln[a/a_c(l)]$. The key idea in deriving (2.7) is that oppositely directed segments $\mathbf{J}(\mathbf{r}) = -\mathbf{J}(\mathbf{r}^*)$ across the diameter $|r - r^*| = a$, multiply the potential U and act as a "discrete derivative" on it. For $T < T_c$, the fugacity falls off exponentially with $y_l \sim e^{-a/\xi_-}$ and the dominant scale $\xi_- \sim (T_c - T)^{-\nu}$ diverges at transition. The helicity modulus at that scale is the vortex coupling with the absorbed scale dependence removed[17] and is also essentially the superfluid-density or spin-wave stiffness $\rho_s \sim K_{l_-} e^{-l_-} \sim |\epsilon|^{\nu}$. Here $dK_{l_-}/dl_- = 0 = dy_{l_-}/dl_-$ as $l_- \to \infty$. One sits on the y_l and K_l inflection point, developing at l_-, and watches the $T < T_c$ solution become unstable as $T \to T_c^-$ and $l_- \to \infty$, with $(K_{l_-}, y_{l_-}) \to (K^*, y^*) = (0.3875, 0.062)$. Numerical solutions have been presented elsewhere[27] with a model[17] $a_c(l)/a \approx (K_l)^x$ for the core, and $x \approx 0.6$ the self-avoiding random walk exponent. This yields $\nu = 0.67$ as the spin-spin correlation exponent,[29] which is also[17(a)] the loop diameter exponent. The random loops for $T > T_c$ have short-range correlations over $\xi_+ \sim |\epsilon|^{-\nu}$, which diverge as $T \to T_c^+$.

We now turn to the anisotropic 3D XY model of (1.1), that is

$$\beta H = -\beta \sum_{\mu = \hat{x}, \hat{y}, \hat{z}} \sum_i \mathcal{J}_\mu \cos \Delta_\mu \theta_i , \tag{2.8}$$

with spin coupling in a layered form $\mathcal{J}_x = \mathcal{J}_y = \mathcal{J}_\parallel$

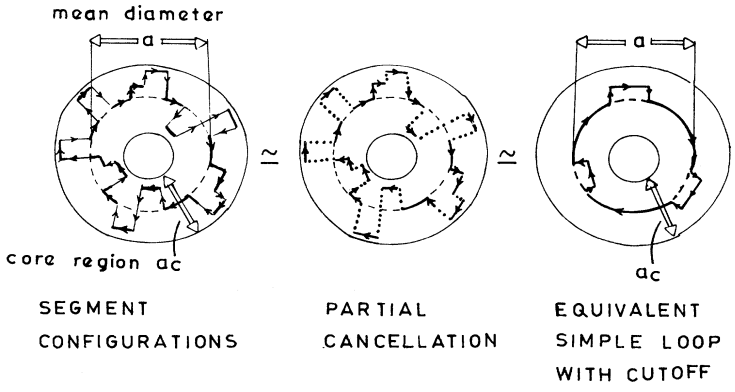

FIG. 2. Effective loop composed of azimuthal current segments as seen at large distances. a, a_c are the mean diameter and core regions of the effective circular loop. Antiparallel radial segments in a hairpinlike excursion within a_c have canceling contributions to the asymptotic potential.

($\mathcal{J}_z=\mathcal{J}_\perp$) within (between) planes. The sites $\{i\}$ are on a lattice of lattice constants $a_x=a_y=a_\parallel$ ($a_z=a_\perp$) within (between) planes, and we later set $a_\perp=a_\parallel=a_0=1$.

In the long-wavelength spin-wave approximation,

$$\beta H \approx \tfrac{1}{2}\beta\mathcal{J}_\parallel \sum_{\mu=\hat{x},\hat{y},\hat{z}} \sum_{\mathbf{q}} (q_\mu a_\mu \sqrt{\mathcal{J}_\mu/\mathcal{J}_\parallel})^2 , \tag{2.9}$$

and the anisotropic coupling constants can be absorbed into new anisotropic lattice constants $a'_\mu=a_\mu(\mathcal{J}_\mu/\mathcal{J}_\parallel)^{1/2}$. This suggests that anisotropic couplings could be irrelevant for critical properties; however, this must be explicitly shown by vortex-loop scaling.

The dual transform[18(b)] of (2.8) to the vortex-loop representation, done in Appendix A, yields[11(a),24(c)]

$$\beta H \simeq \frac{\pi}{2} \sum_{\mathbf{r}\neq\mathbf{r}'} [K_\perp \mathbf{J}_\parallel(\mathbf{r})\cdot\mathbf{J}_\parallel(\mathbf{r}')+K_\parallel J_\perp(\mathbf{r})J_\perp(\mathbf{r}')]\tilde{U}(\mathbf{r}-\mathbf{r}') , \tag{2.10}$$

where the segments $\mathbf{J}_\parallel$ ($J_\perp$) parallel (perpendicular) to the x-y plane couple through $K_\perp$ ($K_\parallel$). Here, as before, $K_\parallel \cong \beta J_\parallel$, $K_\perp \simeq \beta\mathcal{J}_\perp$. The anisotropic interaction is[11(a),24(c)]

$$\tilde{U}(\mathbf{R})=[U(\mathbf{R})-U(0)]=a_\parallel^2 a_\perp \int \frac{d^2q_\parallel dq_\perp}{(2\pi)^3} \frac{4\pi(e^{i\mathbf{q}\cdot\mathbf{R}}-1)}{4-2\cos q_x a_\parallel-2\cos q_y a_\parallel+\gamma_0^{-2}(2-2\cos q_\perp a_\perp)} , \tag{2.11a}$$

and obeys the Green's-function equation

$$(\Delta_\parallel^2+\gamma_0^{-2}\Delta_z^2)\tilde{U}(r)=-4\pi\delta_{\mathbf{r},0} . \tag{2.11b}$$

In coordinate space, changing variables $q_\mu \to q_\mu a'_\mu$, the asymptotic behavior is [$\mathbf{R}=(\mathbf{R}_\parallel,Z)$]

$$U(\mathbf{R}) \simeq \gamma_0 \frac{a_\parallel}{\sqrt{\mathbf{R}_\parallel^2+Z^2/\gamma_0^{-2}(a_\perp/a_\parallel)^2}} = \frac{1}{\sqrt{(R_\parallel/r_0)^2+(Z/a_\perp)^2}} . \tag{2.12}$$

Here a coupling ratio anisotropy parameter has been defined,

$$\gamma_0^{-1} \equiv (K_\perp/K_\parallel)^{1/2} , \tag{2.13}$$

and a related parameter

$$\delta_0 \equiv 1-\frac{K_\perp}{K_\parallel}=1-\gamma_0^{-2} , \tag{2.14}$$

later enters the vortex-loop fugacity. For the isotropic case, the anisotropy parameter $\gamma_0^{-1}=1$ and $\delta_0=0$. For $\gamma_0^{-1}\to 0$, only the $J_\perp J_\perp$ contribution in (2.10) survives, yielding KT pairs in two dimensions, as in Sec. IV. In the second equality of (2.12) a new length scale, considered by Hikami and Tsuneto[28] appears naturally:

$$r_0 \equiv a_\parallel \gamma_0 . \tag{2.15}$$

It suggests that different limiting forms of the potential, and different dominant loops, may enter for in-plane separations $R_\parallel \ll r_0$ and $R_\parallel \gg r_0$.

Since all loop coordinate integrals in the partition function will be scaled in the appropriate lattice constant $\sum_{\mathbf{r}} \to \int d^3r/a_\perp a_\parallel^2$, the lattice constants will drop out on appropriate rescaling $r_\parallel \to a_\parallel r_\parallel$, $z \to z a_\perp$. Thus, we can, without loss of generality, consider $a_\parallel=a_\perp=a_0$, the isotropic lattice. We set $a_0=1$ for convenience, writing it explicitly only where needed to distinguish a length scale.

As in the isotropic case (2.5), we split vortex-loop interactions of $\{\mathbf{J}^{(L)}\}$ into interloop ($L\neq L'$) and intraloop contributions ($L=L'$). By adding and subtracting we also separate out the $L\neq L'$ part of the Hamiltonian, into a contribution that couples all J_μ components through the geometric average of the anisotropic couplings,

$$K_0 \equiv K_\parallel \gamma_0^{-1}=(K_\perp K_\parallel)^{1/2} , \tag{2.16}$$

and the difference, βH_1. Then (2.10) becomes, in the partition function,

$$Z=\sum_{\substack{\{J^{(L)}\}\\ \text{config}}} \exp\left\{-\frac{\pi}{2}K_0 \sum_{L\neq L'} \sum_{\mathbf{r}\neq\mathbf{r}'} \mathbf{J}^{(L)}(\mathbf{r})\cdot\mathbf{J}^{(L')}(\mathbf{r}')U(\mathbf{r}-\mathbf{r}')-\beta H_1\right\} \prod_L y_0^{(L)} . \tag{2.17a}$$

Here the bare Hamiltonian correction βH_1, shown later to scale to zero, is

$$\beta H_1 \equiv \sum_{L\neq L'} \beta H_1^{(L,L')} \equiv \frac{\pi}{2}K_0(1-\gamma_0^{-1}) \sum_{L\neq L'} \sum_{\mathbf{r}\neq\mathbf{r}'} [-\mathbf{J}_\parallel^{(L)}(\mathbf{r})\cdot\mathbf{J}_\parallel^{(L')}(\mathbf{r}')+\gamma_0 J_\perp^{(L)}(\mathbf{r})J_\perp^{(L')}(\mathbf{r}')]U(\mathbf{r}-\mathbf{r}') . \tag{2.17b}$$

The bare fugacity for loop L is determined by the intraloop interaction and segment self-energy, analogous to (2.6),

$$y_0^{(L)}=\exp\left\{-\frac{\pi}{2}\sum_{\mathbf{r}\neq\mathbf{r}'}[K_\perp \mathbf{J}_\parallel^{(L)}(\mathbf{r})\cdot\mathbf{J}_\parallel^{(L)}(\mathbf{r}')+K_\parallel J_\perp^{(L)}(\mathbf{r})J_\perp^{(L)}(\mathbf{r}')]U(\mathbf{r}-\mathbf{r}')-\frac{\pi}{2}U(0)\sum_{\mathbf{r}}K_\perp[\mathbf{J}_\parallel^{(L)}(\mathbf{r})]^2+K_\parallel[J_\perp^{(L)}(\mathbf{r})]^2\right\}. \quad (2.18)$$

For the isotropic case, with the potential energy $U(R)\sim R^{-1}$, the "equipotential" loop is a circle (origin at center of mass), with oppositely directed segments at locations $\mathbf{r}=-\mathbf{r}'$, and at a fixed separation $|\mathbf{r}-\mathbf{r}'|=2r=a$. For the anisotropic case, similarly, from (2.12)–(2.14) the equipotential loop perimeter is

$$\mathbf{r}_\parallel^2+\frac{z^2}{(1-\delta_0)}=(\tfrac{1}{2}a)^2\ , \quad (2.19)$$

which defines an ellipse of major axis $a_L=a$, that for $\gamma_0^{-2}=(1-\delta_0)<1$, is in the x-y plane. As shown in Appendix B, the ellipse is $(x^2/A^2+\eta^2/B^2)=1$ in a x-η coordinate system in the ellipse plane. The major axis is along the x axis and the minor axis along the η axis, making a polar angle α with respect to the z axis. (See multiplane ellipse in Fig. 3.) Comparing with (2.19), the semimajor axis A, and semiminor axis B are

$$A=\tfrac{1}{2}a,\quad B=\tfrac{1}{2}\frac{(1-\delta_0)^{1/2}a}{(1-\delta_0\sin^2\alpha)^{1/2}}\ . \quad (2.20)$$

The α-dependent bare eccentricity $e(\alpha)$, is defined by $B^2=A^2(1-e^2)$, i.e., $e(\alpha)=\delta_0^{1/2}\cos\alpha/(1-\delta_0\sin^2\alpha)^{1/2}$. The minor axis $a[1-e^2(\alpha)]^{1/2}$ is smallest for $\alpha=0$ $[e(0)=\delta_0^{1/2}]$ and largest for $\alpha=\pi/2$, when loops are circular $[e^2(\pi/2)=0]$.

The bare fugacity of loop L (2.18), evaluated in Appendix B, is for diameter a_L, and orientation angle α_L, given by

$$y_0^{(L)}(\alpha)\approx\exp[-\beta E_0(a_L)(1-\delta_0\sin^2\alpha_L)^{1/2}]\ , \quad (2.21)$$

with the circular loop energy[17(a)]

$$\beta E_0(a_L)=\pi^2 K_0\frac{a_L}{a_0}\ln(a_L/a_c)\ . \quad (2.22)$$

For the minimum scale $a_{L=1}=a_\parallel=1$, lattice constant, previous results[17(a)] gave

$$\beta E_0(a_\parallel)=5.631K_0\ . \quad (2.23)$$

Figure 4 shows the plot of bare fugacity (2.21) versus z-axis orientation α with fixed $a=10a_0$ and for $\gamma_0^{-2}=0.005$ $(a<r_0)$ and $\gamma_0^{-2}=0.5$ $(a>r_0)$. The peak is sharper for larger anisotropies. The peaking of the fugacity for $\alpha=\pi/2$ in-plane loops (if $\gamma_0^{-1}<1$) is consistent with the ideas of Friedel in layered superconductors[13] and is easy to understand from (2.8). For a J_z vortex (dual) lattice segment passing through an original-lattice x-y square, there is an angular difference $\Delta\theta=\pi/2$ across each of four x-y square sides, costing a total energy $4K_\parallel$. For a J_x segment passing through a z-y square, the cost is less, $2K_\parallel+2K_\perp=4K_\parallel[1-\delta_0/2]$. Thus for $\gamma_0^{-1}<1$ or $\delta_0>0$ in-plane segments $\mathbf{J}_\parallel$ are favored.

III. SCALING EQUATIONS AT LARGE DISTANCES

The scaling procedure follows the isotropic case,[17] with the (angularly averaged) vortex-loop fugacity $\bar{y}_l$ as the small parameter. The ellipse axis in the x-y plane of the smallest loop defines the general minimum scale $a=e^l$. For $\gamma_0^{-1}<1$, the axis a is the major axis, and $a[1-e^2(\alpha)]^{1/2}<a$, the minor axis. The partition function (2.17) can be written as

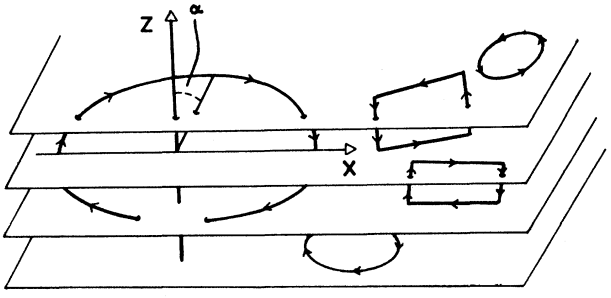

FIG. 3. Various loop configurations. Asymptotically dominant, freely tumbling multiplane ellipses of scale $>r_0$. Finite scale ($<r_0$) rectangular loops cutting a single-plane, which become 2D Kosterlitz-Thouless vortex pairs as planes decouple. Finite scale ($<r_0$) angular constrained, quasi-in-plane loops.

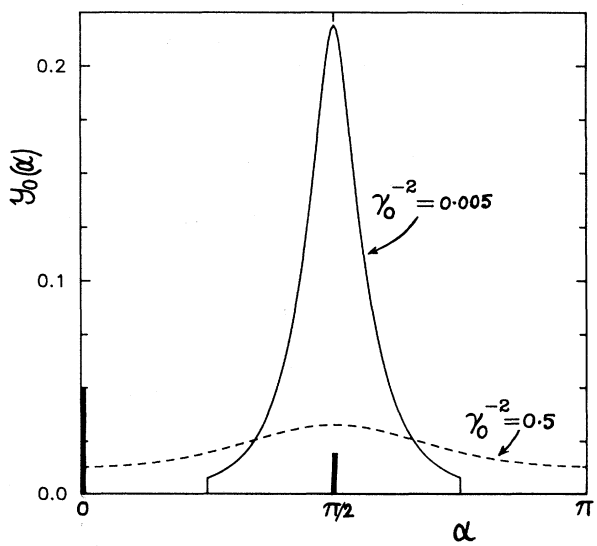

FIG. 4. Bare elliptical-loop fugacity $y_0(\alpha)$ versus z-axis loop-tilt angle α, for loop scale $a=10a_0$, for anisotropic coupling constant ratios $\gamma_0^{-2}\equiv K_\perp/K_\parallel=0.005$ (strong anisotropy, solid line) and $\gamma_0^{-2}=0.5$ (weak anisotropy, dashed line). Solid vertical lines at $\alpha=0$, $\pi/2$ denote quasi-2D excitations, and in-plane loops, respectively, for scales $a<r_0=\gamma_0 a_0$ and strong anisotropy. The wings of the $\gamma_0^{-2}=0.005$ peak are cutoff by the angular constraint of (4.2).

$$Z=\sum_{\substack{\{\mathbf{J}^{(L)}\}\\ \text{config}}}\exp\left[-\frac{\pi}{2}\sum_{L\neq L'}\sum_{\mathbf{r}\neq\mathbf{r}'}K_l\mathbf{J}^{(L)}(\mathbf{r})\cdot\mathbf{J}^{(L')}(\mathbf{r}')U(\mathbf{r}-\mathbf{r}')-\beta H_1\right]\prod_L y_l^{(L)}(\alpha_L)\ , \tag{3.1a}$$

where the correction βH_1 at general scale is, essentially (see Appendix C),

$$\beta H_1=\frac{\pi}{2}K_l(1-\gamma_l^{-1})\sum_{L\neq L'}\sum_{\mathbf{r}\neq\mathbf{r}'}[-\mathbf{J}_\parallel^{(L)}(\mathbf{r})\cdot\mathbf{J}_\parallel^{(L')}(\mathbf{r})+\gamma_l J_\perp^{(L)}(\mathbf{r})J_\perp^{(L')}(\mathbf{r}')]U(\mathbf{r}-\mathbf{r}')\ . \tag{3.1b}$$

Here for the smallest scale ($L=1$) ellipse of scale a, and angle α, $y_l^{(L=1)}(\alpha)\equiv y_l(\alpha)$, and the angular average $\bar{y}_l=\int_0^{\pi/2}d\alpha y_l^{(\alpha)}/(\pi/2)$ is what finally appears. $U(R)\simeq\gamma_l(\mathbf{R}_\parallel^2+Z^2\gamma_l^2)^{-1/2}$, with the renormalized segment-segment coupling K_l absorbing the general scale a. Scaling equations for $K_l,\bar{y}_l$ are found. The difference between the scaling of coefficients in βH_1 and K_l determines the scaling of the renormalized anisotropy γ_l^{-1}, with $\gamma_{l=0}^{-1}=\gamma_0^{-1}=(K_\perp/K_\parallel)^{1/2}$ in the bare case. The general procedure is as follows.

(1) Integrate out the smallest loops, of scales within a, $a+da$. These provide an indirect interaction between larger-loop segments, that is of the same form $\sim U(\mathbf{R})$ as the direct interaction, leading to an incremental "thermal" coupling change, $dK_l\sim -K_l^2\bar{y}_l dl$.

(2) Rescale all explicit scale dependences to be in terms of $a+da$, e.g., minimum-scale volume factors in configuration integrals for the center of mass and relative coordinates of each loop, $a^{-6}\simeq(a+da)^{-6}(1+6dl)$. Demand that the new minimum loop scale is also the new minimum distance of approach of segments on different loops, i.e.,

$$K_l\max(1/R)=K_l a^{-1}=(a+da)^{-1}K_l(1+dl)=(K_l+dK_l)$$

new max $[1/R]$. This gives a "geometrical" change $dK_l\sim K_l dl$, to the coupling that has absorbed the general lattice scale a.

(3) Absorb all explicit $O(dl)$ corrections in redefined fugacities $\bar{y}_{l+dl}$ and couplings K_{l+dl} at the new scale $a+da$.

This yields, as shown in Appendix C, scaling equations of the same form as the isotropic case for the asymptotically dominant elliptical loops

$$\frac{dK_l}{dl}\approx K_l-A_0K_l^2\bar{y}_l\ , \tag{3.2a}$$

$$\frac{d\bar{y}_l}{dl}\approx(6-\pi^2K_lL_l)\bar{y}_l\ , \tag{3.2b}$$

$$\frac{d\beta F_l}{dl}\approx-2\pi\frac{\bar{y}_l}{a^3}\ , \tag{3.2c}$$

with corrections $\sim O(1-\gamma_l^{-1})$. Here the initial values are $K_{l=0}=K_\parallel\gamma_0^{-1}=\sqrt{K_\perp K_\parallel}$;

$$\bar{y}_{l=0}=\left[\frac{2}{\pi}\right]\int_0^{\pi/2}d\alpha\exp[-5.631K_{l=0}(1-\delta_0\sin^2\alpha)^{1/2}]\ ;$$

and $L_l\equiv 1-\ln K_l^{0.6}$, with the same isotropic case core model[17(a)] used, anticipating the result that anisotropy is irrelevant.

In fact, (Appendix C) the renormalized anisotropy γ_l^{-1}, close to the fixed point, scales as

$$\frac{d(1-\gamma_l)^{-1}}{dl}=-(1-\gamma_l^{-1})\ , \tag{3.3}$$

so that the relative correction of βH_1 (2.17b) scales to zero as $(1-\gamma_l^{-1})\sim e^l$. Asymptotically, $\gamma_l^{-1}\to 1$, and the planes are *isotropically coupled*. By contrast, complete layer decoupling would imply $\gamma_l^{-1}\to 0$. The fixed point is 3D, not 2D, consistent with interlayer perturbations of the 2D XY model.[11(e),11(f)]

The physical picture is that the larger loops feel the coupling anisotropy as screened by the nested, smaller, tumbling loops, that average over and weaken the effective anisotropy. The fugacity peaking at $\alpha=\pi/2$ becomes progressively weaker, and elliptical loops become more and more circular at large scale. The fixed-point value of the effective anisotropy is $(\gamma_l^{-1})^*=0$.

The critical coupling $K_{\parallel c}\equiv\bar{T}_c^{-1}=(\mathcal{J}_\parallel/k_BT_c)$ can be evaluated numerically, from changes with temperature variation, in the large-scale flow behavior of (3.2). An approximate expression can be found by linearizing (3.2) about the $l_-=\ln(\xi_-)\to 0$ "fixed points" $(K_{l_-},y_{l_-})=(K^*,y^*)\simeq(0.3875,0.0621)$ when[17(a)]

$$\frac{K_{\parallel c}\gamma_0^{-1}}{K^*}\simeq 1+0.654\left[\frac{\bar{y}_0}{y^*}-1\right]\ . \tag{3.4}$$

The angularly averaged bare fugacity $\bar{y}_0$, is evaluated numerically. For weak anisotropy, $\delta_0\ll 1$, it is[17(c)] approximately

$$\bar{y}_0\simeq e^{-\beta E_0\gamma_0^{-1}}e^{-z}I_0(z),\quad z\equiv\frac{\beta E_0(1-\gamma_0^{-2})}{4\gamma_0^{-1}}\ , \tag{3.5}$$

where $I_0(z)$ is a Bessel function.

An approximate $\bar{T}_c$ versus γ_0^{-2} curve can also be obtained by "approximate self-duality."[24(c)] Going back to (2.10), note that as $T\to T_c$ the $1/R$ potential of ellipses is screened. Dropping the interaction terms, one is left with the self-energy, i.e., $\tilde{U}(R)\to -U(0)$. Neutrality, or (2.4),

$$\left[\sum_{\mathbf{r}}J_\mu^{(L)}(\mathbf{r})\right]^2=\sum_{\mathbf{r}\neq\mathbf{r}}J_\mu^{(L)}(\mathbf{r})J_\mu^{(L)}(\mathbf{r})+\sum_{\mathbf{r}}(J_\mu^{(L)}(\mathbf{r}))^2=0 \tag{3.6}$$

gives the partition function as

$$Z \simeq \sum_{\{J_\mu\}} \exp\left[-\frac{\pi U(0)}{2} \sum_{\mathbf{r}} [\mathbf{J}_\parallel^2(\mathbf{r}) K_\perp + J_\perp^2(\mathbf{r}) K_\parallel] \right] . \quad (3.7)$$

Comparing (3.7) on the dual lattice with (A1) and (A5b) on the original lattice,

$$Z \simeq \sum_{\{n_\mu\}} \exp\left[\frac{-\mathbf{n}_\parallel^2(\mathbf{r})}{2K_\parallel} - \frac{n_\perp^2(\mathbf{r})}{2K_\perp} \right] , \quad (3.8)$$

with $\Delta \cdot \mathbf{n} = 0$, one gets the self-dual condition at T_c of[24(c)]

$$K_{\parallel c} = \frac{\gamma_0}{\sqrt{\pi U(0)}}, \quad \bar{T}_c \equiv K_{\parallel c}^{-1} = \sqrt{\pi U(0)}\,\gamma_0^{-1} , \quad (3.9)$$

where $U(0)$ is defined by (2.11a) and is weakly varying ($\sim \ln \gamma_0$) in γ_0^{-1}.

Figure 5(a) shows a plot (solid line) of the inverse critical coupling or scaled critical temperatures $\bar{T}_c \equiv K_{\parallel c}^{-1}$,

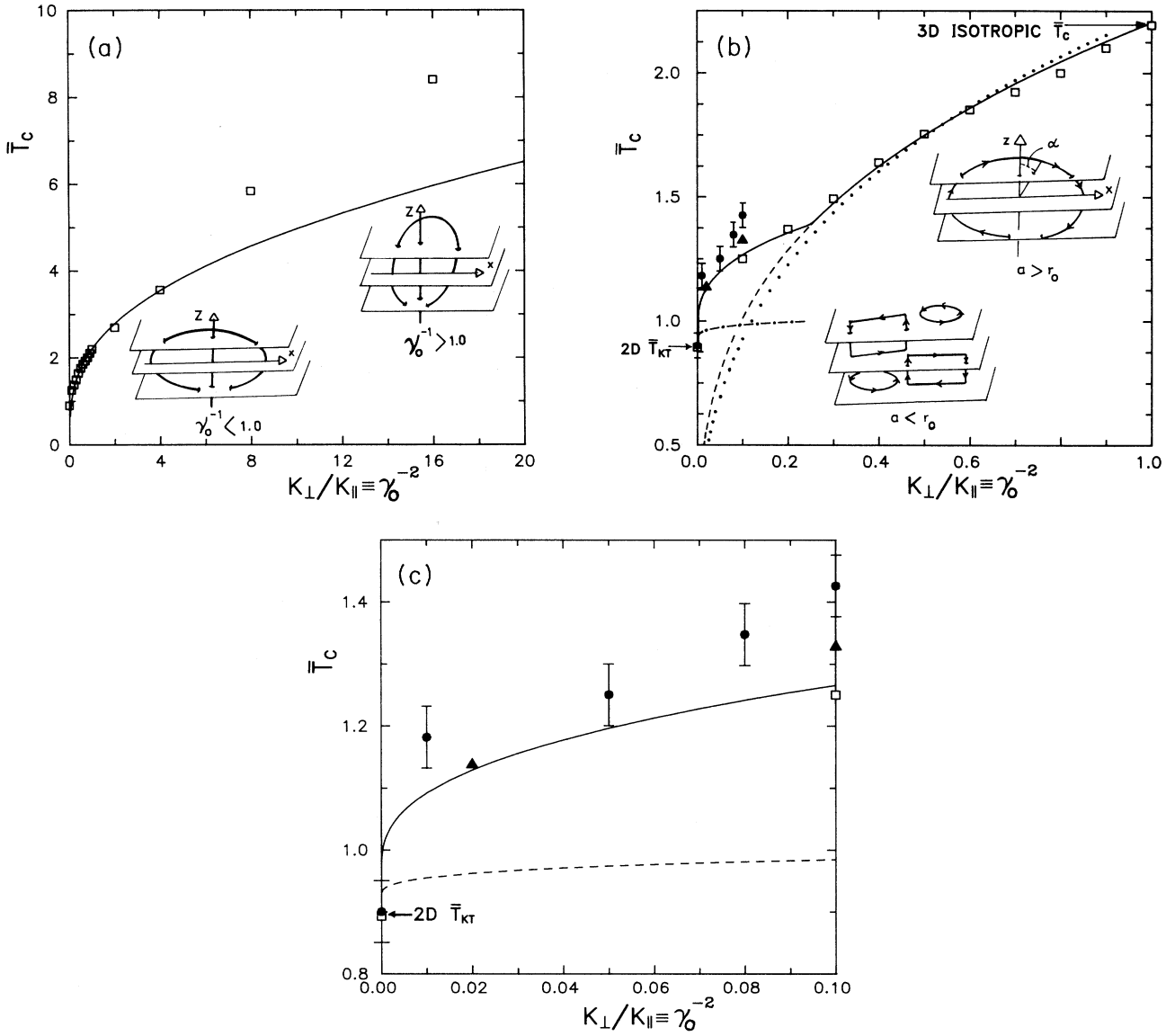

FIG. 5. Dimensionless transition temperature $\bar{T}_c = K_{\parallel c}^{-1}$ versus anisotropic coupling ratio $\gamma_0^{-2} = K_\perp/K_\parallel$, obtained from a temperature that triggers asymptotic changes in (3D) scaling flows. (a) Solid curve $1 < \gamma_0^{-2} < 15$, 3D ellipse-only scaling, with inset showing ellipses for $\gamma_0^{-1} > 1$ (strongly coupled planes) and $\gamma_0^{-1} < 1$ (weakly coupled planes). Symbols are from MC simulations, of Refs. 25(a) and 25(b). (b) $0 < \gamma_0^{-2} < 1$, expanded-scale version of (a). The solid curve is from the (inset) $a < r_0$ quasi-2D excitations and $a > r_0$ multiplane 3D ellipses in the $\gamma_0^{-1} < 0.5$ region and 3D ellipses alone in $\gamma_0^{-1} > 0.5$ region. The dashed line for $\gamma_0^{-1} > 0.5$ is from 3D ellipses only, erroneously extended to all scales. The dotted line is from the approximate self-duality explained in the text. MC data symbols are □ [Ref. 25(a)], ● [Ref. 25(b) and 25(c)], and ▲ [Ref. 10(e)]. The dash-dotted line is the finite-scale unbinding T_{KT} defined in the text. (c) $0 \le \gamma_0^{-2} \le 0.01$, expanded scale version of (b). Dashed line is finite-scale unbinding T_{KT} defined in the text.

found from scaling flow changes of (3.2) versus coupling anisotropy $K_\perp/K_\parallel \equiv \gamma_0^{-2}$ for $0<\gamma_0^{-2}<15$, including strongly coupled planes. For $\gamma_0^{-1}>1$ or $\delta_0=1-\gamma_0^{-2}<0$, the x-y plane ellipse axis that sets the scale, a, is now the smaller or minor axis, with the out-of-plane major axis $a/[1-e^2(\alpha)]$ as shown in the inset of Fig. 5(a). The symbols are the MC data,[25(a)] for $16\times16\times16$ systems, and match theory for γ_0^{-2} not too large.[31]

Figure 5(b) shows the same $\overline{T}_c$ versus γ_0^{-2} plot, but now in the region $0\le K_\perp/K_\parallel<1$. The 3D ellipse-only curve (solid line for $\gamma_0^{-2}>0.25$, dashed line for $\gamma_0^{-2}<0.25$) again agrees with the data, but only up to about $\gamma_0^{-2}\approx0.25$. As the planes decouple, $K_\perp/K_\parallel\to0$, the ellipse-only curve (dashed line) is pushed down to zero. The dotted line is from the approximate self-duality of (3.9). As shown in the next section, the ellipse-only picture breaks down at $\gamma_0^{-2}=0.25$, and finite-scale quasi-2D $a<r_0$ excitations depicted in the inset of Fig. 5(b) must be included, yielding the solid curve for $\gamma_0^{-2}<0.25$. We now turn to the new $a<r_0$ excitations that dominate, for strong anisotropies $\gamma_0^{-1}<0.5$ when the tumbling-ellipse picture breaks down due to angular constraints.

IV. QUASI-2D EXCITATIONS AT FINITE SCALES

The angle-dependent ellipse fugacity (2.21) is peaked for $\alpha=\pi/2$, with in-plane circular loops becoming elliptical as they rotate out of the plane over the range $\pi>\alpha>0$. The tumbling of the loops is necessary for a sampling of the three dimensionality of the system. For the picture to be consistent, however, one must require that the average ellipse minor axis $[a\gamma_0^{-1}/(1-\delta_0\sin^2\alpha)^{1/2}]\le a\gamma_0^{-1}$, must be larger than the minimum (interplane) lattice scale a_0 ($=a_\perp=a_\parallel$). This implies that for a scale small compared to the "Hikami-Tsuneto" (HT) length

$$r_0=a_\parallel\gamma_0\ , \tag{4.1}$$

the elliptical excitations are restricted to oscillations about $\pi/2$ in an angular range $\pi/2\pm\alpha_c$, where

$$\alpha_c\equiv\sin^{-1}\left[\left\{1-\left[\frac{a}{r_0}\right]^2\right\}\Big/\left\{1-\left[\frac{a_\parallel}{r_0}\right]^2\right\}\right]^{1/2}\ . \tag{4.2}$$

The tumbling-ellipse picture cannot be used for scales $a<r_0$, and such loops are constrained to be essentially in plane. For the "forbidden" range of scales $a<r_0$ to be significant, γ_0^{-1} must be small. Since the major axis a is larger than the minor axis (which is $>a_0$), we have $a\ge2a_0$ or $r_0\ge2a_0$, for the constraint of (4.2) to be meaningful.

The $\mathbf{J}_\parallel$ only, strictly in-plane loops of Friedel[13] have zero-energy contribution as $\gamma_0^{-1}\to0$. From (2.10), and the discussion at the end of Sec. II, leading nonzero-energy excitations will have as few $J_\perp$ and as many $\mathbf{J}_\parallel$ segments as possible for a given perimeter. These are effectively rectangular-shaped loops of unit sides $J_\perp=\pm1$ cutting single planes, with an average separation $a<|\mathbf{r}_\parallel-\mathbf{r}'_\parallel|<r_0$, as in Fig. 3. The distribution of $(\mathbf{J}_\parallel,J_\perp)=(J_x,J_y,J_z)$ segment components in existing MC simulations[25] lend some support to this idea of quasi-2D or Hikami-Tsuneto (HT) excitations. Further simulations to check this would be useful. (It should be remembered of course, that these are average shapes; hairpinlike segment excursions about these can, and will, occur.[27])

The smallest rectangular loop has unit sides a_0 in the z direction and sides $2a_0$ in the plane, i.e., $r_0>a>2a_0$. This defines a strong anisotropy regime $\gamma_0^{-2}<0.25$ within which quasi-2D excitations begin to be meaningful. Multiplane elliptical loops are thus effectively suppressed for the scale region $a<r_0$ that is dominated by single-plane HT excitations, and quasi-in-plane loops as in Fig. 3 and the inset of Fig. 5(b). Interestingly, this strong-anisotropy regime estimate is in agreement with the peel-off in Fig. 5(b) of the MC data from the (dashed) ellipse-only transition line.

The potential $U(\mathbf{r}-\mathbf{r}')$ between the vortex-loop segments, in Fourier space, is

$$U(\mathbf{q})=\frac{4\pi}{\mathbf{P}_\parallel^2+\gamma_0^{-2}P_\perp^2}\ , \tag{4.3}$$

where $\mathbf{P}_\parallel^2\equiv4-2\cos q_x a_\parallel-2\cos q_y a_\parallel$, $P_\perp^2\equiv2-2\cos q_z a_\parallel$. For $\gamma_0^{-1}\to0$, one gets the decoupled plane limiting behavior, for $\tilde{U}(R)\equiv U(R)-U(0)$,

$$\tilde{U}(\mathbf{r}-\mathbf{r}')\to-2\delta_{z,z'}U^{(2D)}(\mathbf{r}_\parallel-\mathbf{r}'_\parallel)\ , \tag{4.4}$$

where the 2D interaction potential is, integrating over the Brillouin zone,

$$U^{(2D)}(\mathbf{r}_\parallel)\equiv a_\parallel^2\int\frac{d^2q_\parallel}{(2\pi)^2}2\pi\frac{(1-e^{i\mathbf{q}\cdot\mathbf{r}_\parallel})}{\mathbf{P}_\parallel^2}$$
$$\approx\left[\ln\left[\frac{r_\parallel}{a_0}\right]+\frac{\pi}{2}\right]\ . \tag{4.5}$$

Corrections to the $\ln(R_\parallel)$ potential from expansion of (4.3) are $\sim O((R_\parallel/r_0)^2)$.

From (2.10) and (4.4), the leading order energy contributions of $J_\perp$ segments of rectangular loops for a separation R, with $r_0\gg R\gg a_c$, are given by

$$\beta H\approx\sum_z\left[-\pi K_\parallel\sum_{\substack{\mathbf{r}_\parallel\neq\mathbf{r}'_\parallel\\ L,L'}}J_\perp^{(L)}(\mathbf{r}_\parallel,z)J_\perp^{(L')}(\mathbf{r}'_\parallel,z)\ln\left[\frac{|\mathbf{r}_\parallel-\mathbf{r}'_\parallel|}{a_\parallel}\right]+\frac{\pi^2K_\parallel}{2}\sum_{\substack{\mathbf{r}_\parallel\\ L}}[J_\perp^{(L)}(\mathbf{r}_\parallel,z)]^2\right] \tag{4.6}$$

The $\mathbf{J}_\parallel$ contributions of the long sides, to the energy, become cost-free, as the planes decouple, $\gamma_0^{-1}\to0$. Here loop closure in the component form (3.6) has been used. We see from (4.4) and the large square bracket sum of (4.6), that each plane contributes *independently,* with $z=z'$ components only. In this limit, the quasi-2D excitations dominate, and

planes are effectively decoupled, at *finite* scales $<r_0$. [For asymptotic (3D) scales, the planes are effectively isotropically coupled, as shown earlier.]

As $\gamma_0^{-1}\to 0$, the (circular) loops are restricted to be in-plane only. One can derive 2D KT equations for the coupling and fugacity of in-plane circular loops. The bare Hamiltonian for $\mathbf{J}_\parallel$-only closed loops in a given plane z, is as in (4.6)

$$\beta H(z)=-\pi K_\parallel \gamma_0^{-2}\sum_{\substack{\mathbf{r}_\parallel\neq\mathbf{r}'_\parallel\\ L,L'}}\mathbf{J}_\parallel^{(L)}(\mathbf{r}_\parallel,z)\cdot\mathbf{J}_\parallel^{(L')}(\mathbf{r}'_\parallel,z)\ln\left[\frac{|\mathbf{r}_\parallel-\mathbf{r}'_\parallel|}{a_\parallel}\right]+\frac{\pi^2 K_\parallel\gamma_0^{-2}}{2}\sum_{\substack{\mathbf{r}_\parallel\\ L}}[J_\parallel^{(L)}(\mathbf{r}_\parallel,z)]^2 . \tag{4.7}$$

The scaling argument for nested $J_\parallel$ in-plane loops follows the 3D loop case closely, but with the smallest loops acting as "discrete deviatives" on the logarithmic potential, $\mathbf{J}_\parallel(\mathbf{r})=-\mathbf{J}_\parallel(\mathbf{r}^*)$ for $|\mathbf{r}-\mathbf{r}^*|=a$ across the loop diameter. The dressed coupling and loop fugacity scaling equations are of the 2D KT form, and the transition temperature for in-plane loop blowout is estimated as $K_\parallel\gamma_0^{-2}\sim$const or $\bar{T}_{\rm KT}\sim\mathcal{J}_\parallel\gamma_0^{-2}\ll\bar{T}_c$ the 3D transition temperature, for $\gamma_0^{-2}\ll 1$. Thus, for temperature near T_c, the in-plane loops strongly screen interactions of $\mathbf{J}_\parallel$ segments on the same quasi-2D loop. They also screen $\mathbf{J}_\parallel$ interactions between the top part of a rectangle on one plane and the bottom part of a rectangle on a neighboring plane and help in effective decoupling of the layer excitations on scales $<r_0$. (The direct $\ln R_\parallel$ interaction of the $J_\perp-J_\perp$ sides on one plane would, of course, be unaffected by $J_\parallel$ screening effects, as the $J_\parallel$ and $J_\perp$ segments are orthogonal.)

Now consider corrections to (4.6) from $\mathbf{J}_\parallel$ long sides of HT excitations. Since *all* segment separations R between r_0 and a_0 contribute, we retin the full potential $U(\mathbf{R})$ of (2.12). The segment self-energy contribution $\sim J_\parallel^2$ plus a screened short-ranged interaction, as above, proportional to the length $\sim R_\parallel$ of the long rectangular side, provides an effective linear potential $2\pi Q_0(R_\parallel/a-1)$ between the $J_\perp=\pm 1$ vertical sides, on the same loop. For γ_0^{-1} small dropping the screened interaction energy, the coefficient may be estimated as

$$Q_0=\tfrac{1}{2}K_\parallel U(0)\gamma_0^{-2} . \tag{4.8}$$

For $\gamma_0^{-1}<0.5$ but not tending to zero, the restrictions on angular orientations of the quasi-in-plane loops become less effective, and their screening of the $J_\parallel-J_\parallel$ interaction becomes less. However, the $J_\parallel-J_\parallel$ self-energy with the bare potential again gives a linear potential. The two sides of the rectangle both contribute, and

$$\begin{aligned}\beta H&\approx\pi K_\parallel\gamma_0^{-2}\sum_{x,x'}\frac{r_0}{|x-x'|}\\ &\simeq\pi K_\parallel a_\parallel\gamma_0^{-1}[\ln(K^*)^{-x}][(R_\parallel/a_\parallel)-1] ,\end{aligned} \tag{4.9}$$

where a cutoff in the segment approach, as below (2.7), has been used to incorporate crinkling of the on-average horizontal long sides of the rectangle. The U(0) self-energy terms are absorbed in the core a_c [as in (2.6)] to get the second approximate equality of (4.9). The coefficient Q_0 in this regime is then estimated, with $K^*=0.3875$ and $x=0.6$, as

$$Q_0\simeq 0.284K_\parallel\gamma_0^{-1}a_\parallel . \tag{4.10}$$

We set

$$m(\mathbf{r},z)\equiv J_\perp^{(L)}(\mathbf{r},z) , \tag{4.11}$$

suppressing loop labels. All $\{J_\perp^{(L)}\}$ in (4.6) have the same leading $\ln R_\parallel$ interaction both within ($L=L'$), and between ($L\neq L'$) loops. The effective potential $\sim R_\parallel$ is actually only between $J_\perp=\pm 1$ on the $L=L'$ same loop, but the error made in relaxing this condition ($L\neq L'$ inclusion) is of higher order in the fugacity of loops when doing partition function scaling. Thus, from (4.6) and the above discussion, one has effective vortex "points" $m(r,z)$ with a log-plus linear interaction,

$$\beta H\approx\sum_z\left[-\pi K_\parallel\sum_{\mathbf{r}_\parallel\neq\mathbf{r}'_\parallel}m(\mathbf{r}_\parallel,z)m(\mathbf{r}'_\parallel,z)\ln\left[\frac{|\mathbf{r}_\parallel-\mathbf{r}'_\parallel|}{a_\parallel}\right]+\frac{\pi^2K_\parallel}{2}\sum_{\mathbf{r}_\parallel}m^2(\mathbf{r}_\parallel,z)-\pi Q_0\sum_{\mathbf{r}_\parallel\neq\mathbf{r}'_\parallel}m(\mathbf{r}_\parallel,z)m(\mathbf{r}'_\parallel,z)\left[\frac{|\mathbf{r}_\parallel-\mathbf{r}'_\parallel|}{a_\parallel}-1\right]\right] \tag{4.12}$$

The logarithmic term of (4.12) dominates the effective linear terms right up to scales $a\sim r_0$, for $\gamma_0^{-1}\ll 1$. [For (4.8) the linear term contribution at the largest scale $\sim r_0$ is $Q_0 r_0\sim\gamma_0^{-1}\to 0$, recovering[11(a)] the KT limit.] The standard scaling procedure[7,9] leads to quasi-2D $K_l^{(2D)}, y_l^{(2D)}$ scaling equations for $m=\pm 1$ vortex coupling and vortex *pair* fugacity that reduce to the KT equations as $\gamma_0^{-1}\to 0$:

$$\begin{aligned}\frac{dK_l^{(2D)}}{dl}&=-3A_0K_l^{(2D)}y_l^{(2D)} ,\\ \frac{dy_l^{(2D)}}{dl}&\approx[4-2\pi(K_l^{(2D)}+Q_0e^l)]y_l^{(2D)} ,\end{aligned} \tag{4.13}$$

where $Q_0\equiv[U(0)\gamma_0^{-2}/2]K_0^{(2D)}$, $3A_0=4\pi^3$.

Corrections to $\ln R$ of order $(R/r_0)^2$ have been

dropped, and 3D loops take over for scales beyond r_0. We therefore consider only leading "geometric" scale-dependences of the linear-potential coefficient, $Q_l \approx Q_0 e^l$, ignoring possible screening corrections $\sim y_l^{(2D)}$ to it[10(f)] as higher order, and difficult to estimate consistently.

The 2D bare spin-wave corrected[32] coupling $K_{l=0}^{(2D)} = K_\parallel / [1+(2K_\parallel)^{-1}]$, and pair fugacity $y_{l=0}^{(2D)} = \exp[-\pi^2 K_0^{(2D)}]$, are the inputs for quasi-2D scaling up to $l = l_0 \equiv \ln(r_0/a_0)$. Beyond l_0, the fugacity scales sharply to zero, $y_l^{(2D)} \to 0$, as the linear attractive potential between $m = \pm 1$ vortices starts dominating. This means HT excitations are suppressed as scales increase beyond $a = r_0$. On the other hand, from (4.2), tumbling elliptical loops are angularly constrained, as scales decrease below $a \approx r_0$. The HT single-plane loops convert to multiplane loops at $a = r_0$, which is therefore the natural "handover" scale. The renormalized 2D outputs at $l = l_0$ from (4.13) are the inputs to 3D scaling (3.2):

$$K_{l_0}^{(2D)} = K_{l_0}, \quad y_{l_0}^{(2D)} = \bar{y}_{l_0} . \tag{4.14}$$

This handover choice $l = l_0 = \ln(\gamma_0)$ also has the virtue that in the limit that we ignore thermal renormalizations, and drop fugacity terms, in (3.2), and (4.13) the 2D/3D in-plane couplings $K_{l_0}^{(2D)} \approx K_0^{(2D)} \approx K_\parallel$ and $K_{l_0} \approx K_\parallel \gamma_0^{-1} e^{l_0} \approx K_\parallel$ are continuously matched.

For weak anisotropy $\gamma_0^{-1} > 0.5$, rectangular excitations, that must have long sides $r_0 > 2a_0$, lose their definition, ellipses tumble freely, and (3.2) is used at all scales. The scales where (3.2) and (4.13) are used, are depicted in Fig. 6(a) with the solid line the $a = r_0$ handover boundary crossed at fixed γ_0^{-1}. The renormalized coupling K_l and fugacities y_l versus l are given in Fig. 6(b) for temperatures close to transition.

The transition temperature $\bar{T}_c \equiv K_{\parallel c}^{-1}$ for all γ_0^{-1} is determined as before by the temperature for changes of the asymptotic scaling flows. This yields the solid curve of Fig. 5(b), both for $\gamma_0^{-1} < 0.5$ (2D scaling handed over at l_0 to 3D scaling), and $\gamma_0^{-1} > 0.5$ (3D scaling alone). The transition curve for very strong anisotropies $\gamma_0^{-1} < 0.1$ is as in Fig. 5(c). There is reasonable agreement in Figs. 5(b) and 5(c) between the solid curve and the MC data of Epiney[25(a)] and Baeriswyl *et al.*[25(b)] (□), Chui and Giri[25(c)] (●), and Minnhagen and Olsson[10(e)] (▲). The MC simulations are done on the XY cosine model, with typical MC error bars shown. If (4.10) instead of (4.8) is used for Q_0, it results in a change of only $\sim 2\%$. The quasi-2D finite-scale vortex "unbinding" temperature for the HT excitation $J_\perp = \pm 1$ segments, defined by $\pi K_{l_0}^{(2D)}[T_{KT}(\gamma_0)] \approx 2$ for scaling of (4.13), lies below th $\bar{T}_c$ line, that joins it only at γ_0^{-1}.

For $T > T_c$, the average vortex segment separation ξ_+ at large scales is $\xi_+ = n_v^{-1/3}$, where n_v is the asymptotic single-segment density $n_v = (\bar{y}_l)^{1/2}/a^3$, $a \to \infty$. (Vortex-loop closure implies that for any J_μ there is somewhere on the same loop, a segment $-J_\mu$, so $y_l^{1/2}$ is the relevant *single* segment fugacity.) Figure 7 shows that $\xi_+(T)$ has both critical 3D exponent behavior (solid lines), $\ln(\xi_+) \sim -\nu \ln|\epsilon|$, where $|\epsilon| = [T - T_c(\gamma_0)]/T_c(\gamma_0)$, as well as noncritical quasi-2D behavior (dashed line) $\ln(\xi_+) \sim \tau^{1/2}$, where[33] $\tau \equiv [T/T_{KT}(\gamma_0) - 1]$. We find from numerical fits that $\nu = 0.67$, the 3D XY exponent for $|\epsilon| \to 0$. Note that $\xi_+(T)$ is defined in terms of the *asymptotic* (3D) fugacity. The dashed lines merge towards to $\gamma_0^{-1} = 0$ strictly 2D behavior, away from their respective $T_c(\gamma_0)$'s, consistent with the effective decoupling ideas[10] but here in a *finite*-scale decoupling picture. The noncritical 2D temperature dependences from KT-like unbinding at scales $a < r_0$, comes from the feeding in, by (4.14), of small scales to large scales. We elsewhere find[19] the phase slip resistance R is related to the intersegment separation, and so R also has noncritical quasi-2D and critical 3D behavior.

The 3D critical region $|\epsilon| < |\epsilon_c|$ is estimated by a 5% deviation from the $|\epsilon| \to 0$ straight line of $\ln(\xi_+)$ versus $\ln(|\epsilon|)$, and $|\epsilon_c|$ is plotted (solid line) versus γ_0^{-2} in Fig. 8.

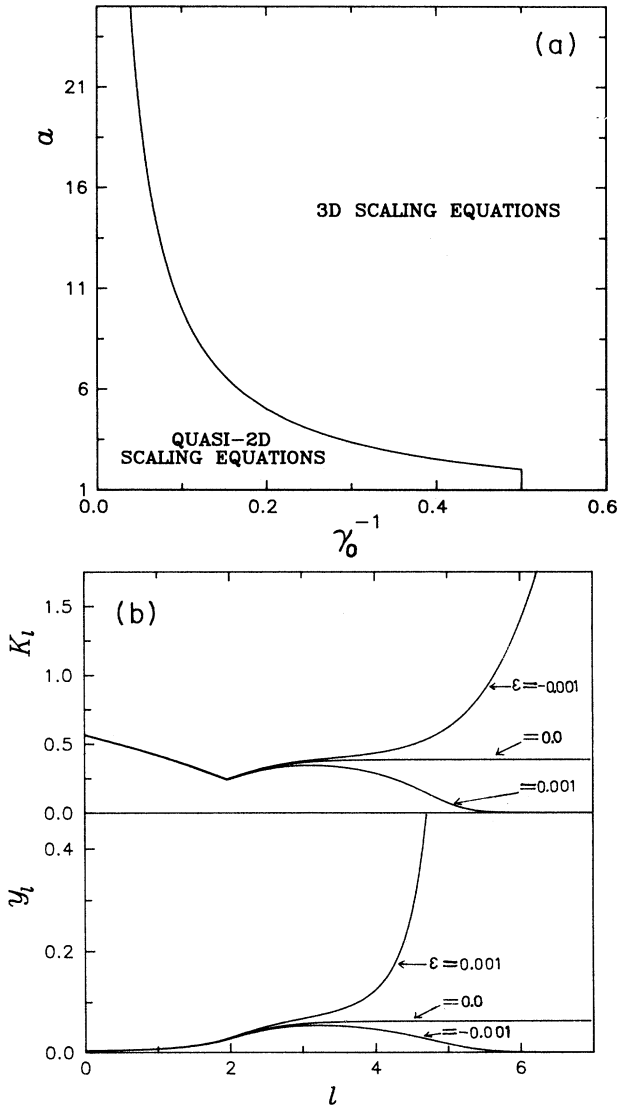

FIG. 6. (a) Scale regions where 2D/3D scaling regions are used, with a handover as the $a = r_0 = \gamma_0 a_0$ line is crossed for constant γ_0^{-1}. (b) Renormalized fugacity y_l and coupling K_l versus scale, $l = \ln(a/a_0)$ for temperatures $\bar{T} = K_\parallel^{-1}$ around the critical value, and for $\gamma_0^{-1} = 0.1414$. Here $\epsilon \equiv (T - T_c)/T_c$.

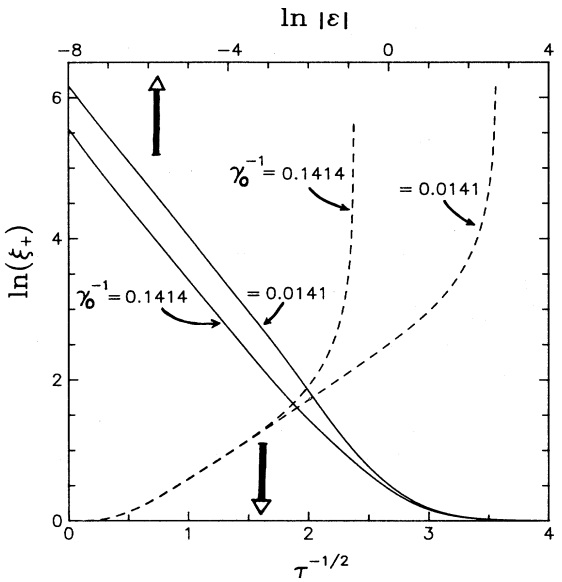

FIG. 7. Logarithm of vortex segment separation $\xi_+(T)$ versus temperature variables for $\bar{T} > \bar{T}_c(\gamma_0)$ and $\gamma_0^{-2} \equiv K_\perp / K_\parallel = 0.0002$, and 0.02. Solid lines are referred to upper horizontal axis $\ln|\epsilon|$, where $|\epsilon| \equiv |[T - T_c(\gamma_0)]/T_c(\gamma_0)|$ and have linear slopes $\nu = 0.67$ for 3D critical region $|\epsilon| \to 0$. Dashed lines refer to the lower horizontal axis $\tau^{-1/2}$, where $\tau = [(\bar{T} - \bar{T}_{KT}(\gamma_0)]/\bar{T}_{KT}(\gamma_0)$, and have (noncritical) KT-like linear behavior, away from its critical region.

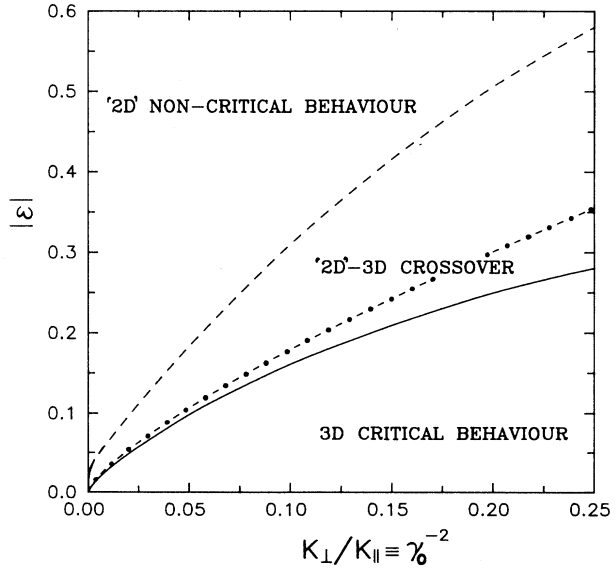

FIG. 8. The solid line showing the 3D critical region boundary of $\epsilon \equiv |[T - T_c(\gamma_0)]/T_c(\gamma_0)| \leq \epsilon_c(\gamma_0)$ versus $\gamma_0^{-2} \equiv K_\perp / K_\parallel$, defined by 5% deviation from 3D exponent behavior. The broad dashed line is the 2D region boundary in $|\epsilon|$ defined by 5% deviation from 2D KT behavior. The dash-dotted line is an estimate $|\epsilon| = \gamma_0^{-1/\nu}$, of the 2D-3D crossover, with $\nu = 0.67$.

For $\gamma_0^{-2} = 2 \times 10^{-4}$ (thallium) $|\epsilon_c| \sim 10^{-3}$, while for $\gamma_0^{-2} \simeq 0.04$(yttrium)$|\epsilon_c| \sim 10^{-1}$. The $|\epsilon|$ for which there is 5% deviation from the linearity of $\ln(\xi_+)$ versus $\tau^{-1/2}$ is also plotted (broad dashed line). There is a 2D-3D crossover region between. A rough bound for $|\epsilon_c|$ is the length crossover condition, $\xi_+ \sim a_0 |\epsilon|^{-\nu} = r_0 = a_0 \gamma_0$, or $|\epsilon|_{\text{cross}} \sim \gamma_0^{-1/\nu}$ (dash-dotted line).

We now briefly comment on similarities and differences with previous work. Minnhagen and co-workers[10] have considered the anisotropic 3D XY model with vorticity-suppressing constraints on alternate planes, either by phases $\theta = 0$ fixed, or with external, local, Shrock-like[26] potentials. By variational and MC simulation methods, they find that (i) the single-plane rectangular vortex loops have $J_z = \pm 1$ unit sides interacting via a

$$2\pi K_\parallel (\ln R_\parallel / a_0) + 2\pi Q_0 (R_\parallel / a_0 - 1)$$

potential and (ii) the bare coefficient $Q_0 \propto \gamma_0^{-1}$. The renormalized finite-temperature linear coefficient of $R_\parallel$ vanishes, $Q_0(T_c) = 0$, at $T = T_c$. (iii) Thus, vortices have a 2D-like, purely $\ln(R_\parallel)$ potential and quasi-2D resistance versus temperature behavior above T_c, i.e., the layers are effectively decoupled for $T > T_c$. (iv) The linear potential terms $\sim R_\parallel$ give rise to an intrinsic critical current, comparable to experiment (but with strength about a factor of 8 larger).

We have studied the anisotropic 3D XY model with no further external constraints on the vortex-loop blowout. We find that (i) for *finite* scales $R_\parallel < r_0$, there are indeed dominant single-plane excitations, with a log-plus-linear interaction obtained from a strong anisotropic limit of the (anisotropic) Biot-Savart potential, but the asymptotic excitations are multiplane loops $\sim \xi_-(T) \sim |\epsilon|^{-\nu}$. (ii) The linear potential bare coefficient Q_0 goes as γ_0^{-2} or γ_0^{-1} in different limits, the latter if screening due to in-plane $J_\parallel$-only loops are neglected. (iii) The quasi-2D finite-scale excitations can feed into and control the (noncritical) loop fugacity, through the scaling equations. This suffices to produce KT-like T dependence in $\xi_+(T)$ governing loop correlations above T_c, even without complete plane decoupling at larger scales. (iv) With lattice constant $a_0 = \xi_\parallel$, the in-plane Ginzburg-Landau length, the ratio of our estimate $2\pi Q_0 = 0.568 \pi K_\parallel \xi_\parallel \gamma_0^{-1}$ to[10] $2\pi Q_0 = \pi^2 \sqrt{2} K_\parallel \xi_\parallel \gamma_0^{-1}$ is about a factor of $\frac{1}{8}$. (v) Even without alternate-plane constraints that suppress loop blowout, one might speculate how a quasi-2D population could arise even at large scales. A current drive I_x will exert, through a Lorentz-like force, a torque on J_y components in the x-y plane, rotating loops to the y-z plane. These loops would become rectangular even on scales larger than r_0, and the $J_z = \pm 1$ sides will be driven outwards, perhaps splitting into single-plane rectangles by fluctuations. The overcoming of the in-plane binding potential (log plus linear) would give rise to a critical current.

V. SUMMARY

We have presented a vortex-loop scaling analysis of the layered 3D XY model, generalizing our previous isotropic

case results. Large loops cutting multiple planes are, on average, elliptical with angle-dependent fugacities peaked for loop orientation in the x-y plane, when the loops are circular. The effective anisotropy seen by the progressively larger loops is progressively smoothed by the smaller, tumbling loops, driving the effective anisotropy to zero. The asymptotic scaling equation behavior for renormalized coupling and fugacity is that of an isotropic model with bare vortex-loop coupling that is the geometric mean $K_0 \equiv \sqrt{K_\perp K_\parallel} \equiv K_\parallel \gamma_0^{-1}$ of the actual couplings. Thus, critical exponents are unchanged: anisotropy is irrelevant.

The transition temperature $\bar{T}_c = k_B T_c / \mathcal{J}_\parallel \equiv K_{\parallel c}^{-1}$ versus coupling ratio $K_\perp / K_\parallel \simeq \mathcal{J}_\perp / \mathcal{J}_\parallel \equiv \gamma_0^{-2}$ from multiplane elliptical loops alone is in good agreement with MC data points in the region $0.25 < K_\perp / K_\parallel < 15$. In the high-anisotropy regime, $\gamma_0^{-2} < 0.25$, the elliptical loops are restricted to a range of angles about the plane and become strictly in-plane, as $\gamma_0^{-1} \to 0$. A new population of long rectangular loops of unit sides $J_\perp = \pm 1$ cutting single planes become important for in-plane scales $R_\parallel < r_0 = a_\parallel \gamma_0$, beyond which they are improbable, and the asymptotically dominant multiplane loops take over. Thus, for $\gamma_0^{-1} \ll 0.5$ or $r_0 \gg 2a_\parallel$, the lattice planes fluctuate independently, and are effectively decoupled, over finite scales $< r_0$. The in-plane potential for $J_\perp = \pm 1$ sides of these quasi-2D excitations is logarithmic, $\sim K_0 \ln R_\parallel$, with small linear $\sim R_\parallel$ corrections. This yields KT-like quasi-2D scaling equations for scales $< r_0$, with the quasi-2D renormalized coupling and fugacity feeding in as inputs into the 3D scaling equations. With the inclusion of finite-scale quasi-2D inputs, the transition temperature T_c, found by a change in asymptotic behavior, matches the MC data in the high-anisotropy regime, $\gamma_0^{-2} \leq 0.25$, and T_c is driven to the KT transition temperature (and not to zero) as the planes decouple.

With the scaling equations in the high anisotropy, finite scale $< r_0$ regime, one can now calculate[19] renormalized stiffness constant or helicity modulus–superfluid density, quasi-2D resistance behavior, and nonlinear I-V characteristics. These could have relevance for recent work on layered high-T_c superconductors.[5,6] Using the anisotropic scaling equations, one might also examine the problem of quantum fluctuations in capacitive Josephson arrays,[34] granular superconducting films at low temperatures,[35] and high-T_c models[15] that map onto an (anisotropic) classical (2+1)D XY model.

In conclusion, a vortex loop scaling analysis of the anisotropic 3D XY or planar ferromagnet has been presented, which may have relevance for other problems of current interest.

ACKNOWLEDGMENTS

It is a pleasure to thank J. Banavar, J. van Himbergen, P. Minnhagen, and T. Schneider for valuable conversations. B.C. thanks UGC (India) for financial support.

APPENDIX A: DUAL TRANSFORM OF THE ANISOTROPIC 3D XY MODEL

The dual transformation[18(b)] extracts topological excitations and their long-range interactions from nearest-neighbor Hamiltonians and their symmetries. The transform, applied to the partition function of the anisotropic 3D XY model, follows the isotropic case closely. The results are as elsewhere[11(a),24] with derivation sketched here for completeness. We take at an intermediate stage $a_\mu = a_0 = 1$ a cubic lattice, without loss of generality, as noted in the text. The number of lattice sites is $N \equiv N_x \times N_y \times N_z$.

(i) *Fourier expand the Boltzmann factor, and integrate:*

$$
\begin{aligned}
Z &= \prod_i \int_{-\pi}^{\pi} \frac{d\theta_i}{2\pi} \exp\left[\sum_\mu \sum_i \beta \mathcal{J}_\mu \cos \Delta_\mu \theta_i \right] \\
&= \prod_i \int_{-\pi}^{\pi} \frac{d\theta_i}{2\pi} \sum_{\{n_{\mu,i}\}} \exp[V(\{n_{\mu,i}\})] \exp\left[i \sum_{\mu,i} n_{\mu,i} \Delta_\mu \theta_i \right] \\
&= \sum_{\{n_{\mu,i}\}} \exp[V(\{n_{\mu,i}\})] \prod_i \delta_{\Delta \cdot \mathbf{n}_i, 0}
\end{aligned}
\tag{A1}
$$

Here $n_{\mu,i} = 0, \pm 1, \pm 2, \ldots, \pm\infty$ ($\exp[V(\{n_{\mu,i}\})]$) are the Fourier labels (Fourier coefficients), with $n_{\mu,i}$ as integers, reflecting the $\Delta\theta \to \Delta\theta + 2\pi$ symmetry of the cosine Hamiltonian. Direction labels are $\mu = \hat{x}, \hat{y}, \hat{z}$, or 1,2,3. The Fourier coefficients will tend to increase, with decreasing temperature, which is inconvenient for a low-T calculation. Although $\Delta \cdot \mathbf{n}_i = 0$, we will use the phrase "vortex loops" only for dual-lattice variables $\mathbf{J}(r)$, with $\Delta \cdot \mathbf{J}(r) = 0$, which appear later, and whose (renormalized) loop fugacity is the small expansion parameter, at low temperatures.

(ii) *Satisfy the constraint as an identity.* Introducing dual lattice variables $\mathbf{N}(i)$, with $N_\lambda(i) = 0, \pm 1, \pm 2, \ldots, \pm\infty$ on a dual cubic lattice displaced from the original lattice by $(\frac{1}{2}, \frac{1}{2}, \frac{1}{2})$, the original lattice $\mathbf{n}_i$ can be written as the curl,

$$
n_{\mu,i} = \sum_{\nu,\lambda=1,2,3} \epsilon_{\mu\nu\lambda} \Delta_\nu N_\lambda(i) \, , \tag{A2}
$$

where $\epsilon_{\mu\nu\lambda} = +1$ (-1) for cyclic (noncyclic) coordinate direction labels, and zero for any two coordinates directions that are equal. Thus $\Delta \cdot \mathbf{n} = \Delta \cdot (\Delta \times \mathbf{N}) = 0$. Then (A1) becomes

$$Z=\sum_{\{N_\lambda(i)\}} e^{V\{[(\epsilon\Delta N)_{\mu,i}]\}} . \tag{A3}$$

(iii) *Use the Poisson summation formula.* This gives new integer variables $\{\mathbf{J}(\mathbf{r})\}$ (vortex-loop segments) and continuum variables $\{\boldsymbol{\phi}(\mathbf{r})\}$ ("spin waves")

$$Z=\prod_\lambda \int_{-\infty}^{\infty} d\phi_\lambda(r) \sum_{\{J_\mu(\mathbf{r})\}} \exp(V\{[(\epsilon\Delta\phi)_{\mu,i}]\})\exp\left[2\pi i \sum_{\mathbf{r}} \boldsymbol{\phi}(\mathbf{r})\cdot\mathbf{J}(\mathbf{r})\right] , \tag{A4}$$

with $\Delta\cdot\mathbf{J}(\mathbf{r})=0$ by gauge invariance $\boldsymbol{\phi}(\mathbf{r})\to\boldsymbol{\phi}(\mathbf{r})+\Delta\chi(\mathbf{r})$ and integration over $\chi(\mathbf{r})$. So far, everything is *exact.*

(iv) *Evaluate the Fourier coefficient in low-T approximation.* We have $e^{V(\{x_{\mu,i}\})}=\prod_{\mu,i} e^{V(x_{\mu,i})}$, and the inverse Fourier transform gives the Fourier coefficient or weight factor as

$$\begin{aligned} e^{V(x_{\mu,i})} &= \int_{-\pi}^{\pi}\frac{d\theta_i}{2\pi}\int_{-\pi}^{\pi}\frac{d\theta_{i+\mu}}{2\pi} e^{\beta\mathscr{J}_\mu\cos\Delta_\mu\theta_i} e^{i(x_{\mu,i})\Delta_\mu\theta_i} \\ &\equiv I_{x_{\mu,i}}(\beta\mathscr{J}_\mu)=I_0(\beta\mathscr{J}_\mu)\exp[\ln(\{I_x/I_0-1\}+1)] , \end{aligned} \tag{A5a}$$

where $I_n(x)$ is a modified Bessel function of imaginary argument. For $(\beta\mathscr{J}_\mu)^{-1}\ll 1$

$$e^{V(x_{\mu,i})}\simeq I_0(\beta\mathscr{J}_\mu)e^{-x_{\mu,i}^2/2K_\mu} \tag{A5b}$$

with $K_\mu=K_\mu(\beta\mathscr{J}_\mu)\approx\beta\mathscr{J}_\mu$ at low temperatures. The behavior of $K_\mu(\beta\mathscr{J}_\mu)$ near T_c is discussed later.

(v) *Integrate over continuous variables* $\phi_\lambda(r)$. In Fourier space, the weight factor in (A4), using (A5b), is given by

$$\begin{aligned} \exp[V(\{\epsilon\Delta\phi\})] &= \exp\left[\sum_{\mu,i} V\{[(\epsilon\Delta\phi)_{\mu,i}]\}\right] \\ &\simeq \exp\left[-\sum\frac{[\epsilon\Delta\phi_{\mu,i}]^2}{2K_\mu}\right] \\ &= \exp\left[-\sum_{\mathbf{q}}\frac{|\mathbf{P}(\mathbf{q})\times\boldsymbol{\phi}(\mathbf{q})|^2}{2K_\mu}\right] , \end{aligned} \tag{A6}$$

where $|P_\mu(\mathbf{q})|^2\equiv 2-2\cos q_\mu a_\mu$ and a_μ are lattice constants. Changing variables

$$\phi_\mu\equiv(K_\mu)^{-1/2}\phi'_\mu,\quad P_\mu\equiv(K_\mu)^{-1/2}P'_\mu , \tag{A7}$$

we have

$$\exp V\{[(\epsilon\Delta\phi)_{\mu,i}]\}=\exp\left[-\sum_{\mathbf{q},\mu}\frac{|(\epsilon P'\phi')_{\mu,i}|^2}{2K_xK_yK_z}\right]=\exp\left[-\sum\frac{|\mathbf{P}'|^2|\boldsymbol{\phi}'(q)|^2}{2K_\perp K_\parallel^2}\right] , \tag{A8}$$

where $K_x=K_y=K_\parallel$, $K_z=K_\perp$ for layered couplings and a gauge $\mathbf{P}'\cdot\boldsymbol{\phi}'(\mathbf{q})=0$ is chosen. Using (A8) in (A4), and integrating over $\phi'(\mathbf{q})$, the partition function in Fourier space is

$$Z\simeq\sum_{\{J\}}\exp\left[-\frac{\pi}{2}\sum_{\mathbf{q},\mu}\frac{K_\perp K_\parallel^2}{K_\mu}\frac{|J_\mu(\mathbf{q})|^2}{|P'_\mu(\mathbf{q})|^2}\right] , \tag{A9}$$

where the term that has $|\mathbf{P}'(q)|=0$ is excluded, and irrelevant factors are dropped.

The anisotropic vortex-loop model partition function is then, with $(J_x,J_y)=\mathbf{J}_\parallel$, $J_z=J_\perp$

$$Z=\sum_{\{J\}}\exp\left[-\frac{\pi}{2}\sum_{\mathbf{r}\neq\mathbf{r}'}(K_\perp\mathbf{J}_\parallel(\mathbf{r})\cdot\mathbf{J}_\parallel(\mathbf{r}')+K_\parallel J_\perp(\mathbf{r})J_\perp(\mathbf{r}'))\tilde{U}(\mathbf{r}-\mathbf{r}')\right] . \tag{A10}$$

The potential is the lattice Green's function, with

$$U(\mathbf{R})=a_\perp a_\parallel^2\int\frac{d^2q_\parallel\,dq_z}{(2\pi)^3}\frac{e^{i\mathbf{q}\cdot\mathbf{R}}4\pi}{4-2\cos(q_xa_\parallel)-2\cos(q_ya_\parallel)+[2-2\cos(q_za_\perp)]\gamma_0^{-2}} . \tag{A11}$$

Here $\gamma_0^{-2}\equiv K_\perp/K_\parallel$, and we define $\tilde{U}(\mathbf{R})\equiv[U(\mathbf{R})-U(0)]$, i.e., $\tilde{U}(\mathbf{q})=[U(\mathbf{q})-\delta_{|\mathbf{P}'|,0}\sum_{\mathbf{q}}U(\mathbf{q})/N]$.

With $\{\mathbf{J}\}=(\{\mathbf{J}^{(L)}\})$ vortex segments are labeled by the loop (L) to which they belong, and there is closure for each loop separately, $\Delta\cdot\mathbf{J}^{(L)}(\mathbf{r})=0\forall L$. The constant $U(0)$ terms by closure $\sum_{\mathbf{r}}J_\mu^{(L)}(\mathbf{r})=0\forall\mu$ of (3.6) go into the fugacity of (2.6) and get absorbed into the core size[16,17] a_c. Separating $L\neq L'$ interloop segment interaction energies,

$$Z=\sum_{\{J_\mu^{(L)}(\mathbf{r})=0,\pm1\}}\exp\left[-\frac{\pi}{2}\sum_{L\neq L'}\sum_{\mathbf{r}\neq\mathbf{r}'}[K_\perp\mathbf{J}_\parallel^{(L)}(\mathbf{r})\cdot\mathbf{J}_\parallel^{(L')}(\mathbf{r}')+K_\parallel J_\perp^{(L)}(\mathbf{r})J_\perp^{(L')}(\mathbf{r}')]U(\mathbf{r}-\mathbf{r}')\right]\times\prod_L y_0^{(L)}\ , \tag{A12}$$

where $y_0^{(L)}$ is the fugacity from the $L=L'$ intraloop segment interaction, as in (2.6) and evaluated in Appendix B. From (A10), with $\mathbf{R}=(\mathbf{R}_\parallel,Z)$ and r_0 as in (2.13) and (2.15),

$$U(\mathbf{R})\simeq\frac{1}{\sqrt{(\mathbf{R}_\parallel/r_0)^2+(Z/a_\perp)^2}}\ , \tag{A13}$$

asymptotically. More precisely $U(\mathbf{R})$ is the 3D lattice Green's function,

$$(\Delta_\parallel^2+\gamma_0^{-2}\Delta_\perp^2)\tilde{U}(\mathbf{R})=-4\pi\delta_{\mathbf{R},0}\ . \tag{A14}$$

Z can be written as in (2.17) of the text, by adding and subtracting terms,

$$Z=\sum_{\{J_\mu^{(L)}\}}\exp\left[-\frac{\pi}{2}\sum_{L\neq L'}\sum_{\mathbf{r}\neq\mathbf{r}'}K_0\mathbf{J}^{(L)}(\mathbf{r})\cdot\mathbf{J}^{(L')}(\mathbf{r}')U(\mathbf{r}-\mathbf{r}')-\beta H_1\right]\prod_L y_0^{(L)}\ . \tag{A15}$$

Here $K_0\equiv K_\parallel\gamma_0^{-1}$ and the bare anisotropic correction term [of (3.1b)] can be written as

$$\beta H_1\equiv\frac{\pi}{2}K_0(1-\gamma_0^{-1})\sum_{L\neq L'}\sum_{\mathbf{r}\neq\mathbf{r}'}[-\mathbf{J}_\parallel(\mathbf{r})\cdot\mathbf{J}_\parallel(\mathbf{r}')+\gamma_0 J_z(\mathbf{r})J_z(\mathbf{r}')]U(\mathbf{r}-\mathbf{r}')\ . \tag{A16}$$

We need a connection between the vortex coupling $K_\parallel$ and the temperature T_c, valid near the transition temperature $T=T_c$. From (A5), as mentioned, $K_\parallel\simeq\beta\mathcal{J}_\parallel$ for $T\to0$, and the bare vortex coupling is the original cosine coupling. The cosine interaction supports both vortices and spin waves, and for low temperatures, $T\ll T_c$, there will be (long-wavelength) spin-wave corrections as in two dimensions[32] to the bare (even short-distance) vortex coupling, since vortices are extended objects.

Working with[36] a truncated version of (A5) in (A1), and restricting $\mathbf{n}$ to three values $n_{\mu i}=0,\pm1$ with $\boldsymbol{\Delta}\cdot\mathbf{n}=0$,

$$Z\simeq\sum_{\{n_\mu=0,\pm1\}}\exp\left[-\sum_i\mathbf{n}_i^2/2K'\right]\ , \tag{A17}$$

in the isotropic case. Comparing this with the first three coefficients of the cosine weight factor yields[36] a nonlinear relation between K' and $\beta\mathcal{J}$. However, the derivation of (A4) from (A1) requires a sum over all integer values $n_{\mu,i}=0,\pm1,\pm2,\ldots\pm\infty$ in an intermediate step. It is the final "vortex" variable $J_\mu(i)$ (and not the intermediate variable $\mathbf{n}_i$) that is eventually restricted to its smallest values $0,\pm1$ in a leading-order vortex-fugacity expansion. It is not obvious what the relation $K(\beta\mathcal{J})$ will be in such a case. The spin-wave stiffness must be renormalized by the vortices; the short-distance force between vortices is renormalized by spin waves. A self-consistent scheme is required, in general. We appeal, therefore to a physical argument near T_c.

In two dimensions, the long-wavelength spin-wave stiffness is nonzero at T_{KT}^-, spin waves are well-defined right up to transition, and the low-T expansion gives a good description[36] of the actual spin-wave renormalization of the bare vortex-vortex coupling.

In three dimensions, however, the long-wavelength spin-wave stiffness vanishes[23] at T_c as a power of T_c-T, spin waves are less well-defined at the transition, and any spin-wave corrections must go as a power of T_c-T, implying the bare vortex-type coupling is again valid with $K\simeq\beta\mathcal{J}$ near T_c. This assumption was made earlier[17] and gave good results for the critical coupling; here it is assumed to hold also in the anisotropic case, $K_\parallel\simeq\beta\mathcal{J}_\parallel$, $K_\perp\simeq\beta\mathcal{J}_\perp$. The good agreement in this paper between the critical coupling from the MC simulation of the cosine model $[\beta\mathcal{J}_{\parallel c}(\gamma_0)]$ and the vortex scaling $[K_{\parallel c}(\gamma_0)]$ lends indirect support to this physical picture.

APPENDIX B: LOOP SELF-ENERGIES FROM INTRALOOP INTERACTIONS

The large-scale excitations are a continuous closed line of vortex segments having the same potential, $U(\mathbf{r}-\mathbf{r}')=U(2r)$ between opposite $\mathbf{r}=-\mathbf{r}'$ segments. In the isotropic case, $(2\mathbf{r})^2=a^2$ represents a circle $r=(a/2)$. In the anisotropic case, we set (with $a_\perp=a_\parallel=a_0=1$), from (2.12),

$$\mathbf{r}_\parallel^2+z^2/(1-\delta_0)=(a/2)^2,\quad \delta_0=1-\gamma_0^{-2}=1-(K_\perp/K_\parallel)\ , \tag{B1}$$

representing an ellipse. For a coordinate system with x-η in the plane of the ellipse, $x^2/A^2+\eta^2/B^2=1$, where A,B are the semimajor (along x) and semiminor (along η) axes. For a segment $\mathbf{J}$ making an angle ϕ with respect to the x (major) axis, $x=A\cos\phi$ and $\eta=B\sin\phi$. With α the polar or ellipse tilt angle between η and Z, the coordinates are $z=\eta\cos\alpha$ and $y=\eta\sin\alpha$. Substituting into (B1), the semimajor and semiminor axes are

$$A=\frac{a}{2},\quad B=\frac{a}{2}\frac{(1-\delta_0)^{1/2}}{(1-\delta_0\sin^2\alpha)^{1/2}}\equiv[1-e^2(\alpha)]^{1/2}A\ . \tag{B2}$$

Here a is the ellipse scale in the x-y plane and is the major axis for $\delta_0>0$, $\gamma_0^{-1}<1$. In-plane $\alpha=\pi/2$ loops are

circular, of diameter a, while ellipse eccentricity $e(\alpha)$ is largest for vertical, $\alpha=0$ loops, when $\eta=z$, $B=(a/2)(1-\delta_0)^{1/2}$ and $e(0)=\delta_0^{1/2}$. For $\gamma_0^{-1}=(K_\perp/K_\parallel)^{1/2}\to 0$, loops get squeezed to higher eccentricities. The ellipse distance from the origin is $(x^2+y^2+z^2)^{1/2}=A(1-e^2\sin^2\phi)^{1/2}$.

With this parametrization,

$$[\gamma_0^{-1}U(r-r')]^2=(x-x')^2+(y-y')^2+\frac{(z-z')^2}{(1-\delta_0)}=\left[\frac{a}{2}\right]^2[2(1-\cos(\phi-\phi')] , \tag{B3}$$

with the form on the right as it appears[17,27] in the isotropic case.

The topological current segments can also be parametrized in terms of α and ϕ. If ψ is the angle between the $\mathbf{J}$ direction and the x axis in the x-η plane, then, in the general x-y-z frame, $\mathbf{J}=(\cos\psi,\sin\psi\sin\alpha,\sin\psi\cos\alpha)$. Since $\mathbf{J}$ is tangential to the elliptical curve, $\tan\psi=d\eta/dx=-B\cot\phi/A$. Then

$$\cos\psi=\frac{1}{\sqrt{1+(B^2/A^2)\cot^2\phi}} , \qquad \sin\psi=-\frac{B}{A}\frac{\cot\phi}{\sqrt{1+(B^2/A^2)\cot^2\phi}} . \tag{B4}$$

The fugacity, for a loop $a_L=a$, $\alpha_L=\alpha$ is

$$y_0^{(L)}\equiv e^{-\beta E_0^{(L)}} , \tag{B5a}$$

where

$$\beta E_0^{(L)}=\frac{\pi}{2}\sum_{r\neq\mathbf{r}}[K_\perp\mathbf{J}_\parallel(\mathbf{r})\cdot\mathbf{J}(\mathbf{r}')+K_\parallel J_\perp(\mathbf{r})J_\perp(\mathbf{r}')]U(\mathbf{r}-\mathbf{r}')+\frac{\pi}{2}U(0)\left[K_\parallel\sum J_\perp^2(\mathbf{r})+K_\perp\sum\mathbf{J}_\parallel^2(\mathbf{r})\right] . \tag{B5b}$$

The energy can be written as (temporarily suppressing the $U(0)$ self-energy term)

$$\beta E_0^{(L)}\approx\pi^2 a\gamma_0\int_0^{2\pi}\frac{d\phi}{2\pi}\int_0^{2\pi}d\phi'\left[\frac{K_\perp[\sin^2\phi+(1-e^2)\sin^2\alpha\cos^2\phi]+K_\parallel(1-e^2)\cos^2\alpha\cos^2\phi}{\sqrt{2[1-\cos(\phi-\phi')]}}\right]\frac{(1-e^2\sin^2\phi)}{(1-e^2\cos^2\phi)} , \tag{B6}$$

where we have, as in the isotropic case,[17] made a sharp-peaking $\phi\approx\phi'$ approximation in the current-current products.

With a cutoff a_c'/a on the $\phi-\phi'$ angular integration and absorbing constants of integration and $\pi U(0)$ self-energies, etc., into the final core size a_c, as mentioned in the text, the isotropic case loop energy is[17]

$$\beta E_0(a)=\pi^2 K_\parallel\frac{a}{a_0}\ln[a/a_c(l)] . \tag{B7}$$

Doing the ϕ integration[37(a)] in (B7), the anisotropic case fugacity is angle dependent

$$y_0^{(L)}(\alpha)=\exp[-\beta E_0(a)(1-\delta_0\sin^2\alpha)^{1/2}] , \tag{B8}$$

as in (2.21) of the text. Here we have dropped corrections $\sim[1-e^2(\alpha)]^{1/2}\{[1-e^2(\alpha)]^{1/2}-1\}$, which are small in all relevant limits $\alpha\sim\pi/2$ for all δ_0, and $\delta_0\to 0$, $\delta_0\to 1$ for all α.

APPENDIX C: VORTEX-LOOP SCALING

At a general minimum scale, $a\equiv a_0 e^l$ the partition function of (2.17) can be written as a sum of an isotropic current scalar product part, plus an anisotropic correction $[\mathbf{J}_\parallel=(J_x,J_y), J_\perp=J_z]$,

$$Z=\sum_{\substack{\{J_\mu^{(L)}\}\\ \text{config}}}\exp\left[-\frac{\pi}{2}\sum_{L\neq L'}\sum_{\mathbf{r}\neq\mathbf{r}'}K_l\mathbf{J}^{(L)}(\mathbf{r})\cdot\mathbf{J}^{(L')}(\mathbf{r}')U(\mathbf{r}-\mathbf{r}')-\beta H_1\right]\prod_L y_l^{(L)}(\alpha_L) , \tag{C1}$$

where the (A16) correction term βH_1 can be written in a symmetrized form

$$\beta H_1\equiv\frac{\pi}{2}K_l(1-\gamma_l^{-1})\sum_{L\neq L'}\sum_{\mathbf{r}\neq\mathbf{r}'}[\tfrac{1}{2}(\gamma_l-1)g_l\mathbf{J}^{(L)}(\mathbf{r})\cdot\mathbf{J}^{(L')}(\mathbf{r}')+\tfrac{1}{2}(\gamma_l+1)\mathbf{J}_\perp^{(L)}(\mathbf{r})\otimes\mathbf{J}_\perp^{(L')}(\mathbf{r}')]U(\mathbf{r}-\mathbf{r}') . \tag{C2}$$

The coupling K_l has absorbed a minimum length scale a, as mentioned in the text. We here define a product $\mathbf{J}\otimes\mathbf{J}\equiv J_\perp J_\perp-\mathbf{J}_\parallel\cdot\mathbf{J}_\parallel=\sum_{\mu\nu}J_\mu J_\nu A_{\mu\nu}$ with $A_{zz}=+1$, $A_{xx}=A_{yy}=-1$, while, of course, $\mathbf{J}\cdot\mathbf{J}=J_\perp J_\perp+\mathbf{J}_\parallel\cdot\mathbf{J}_\parallel=\sum_\mu J_\mu J_\mu$. Here g_l is a coupling constant that may be generated by scaling with the bare value $g_0=1$. The bare fugacity $y_0^{(L)}$ is as defined in (2.21), and the bare coupling in the main part of the Hamiltonian is $K_{l=0}=\sqrt{K_\perp K_\parallel}$, the geometric mean of the anisotropic couplings. Here the interaction $U(\mathbf{r}-\mathbf{r}')$ satisfies the equation at general minimum scale a,

$$(\Delta_\parallel^2+\gamma_l^{-2}\Delta_z^2)U(\mathbf{r})\equiv\mathbf{D}^2U(\mathbf{r})=-4\pi\delta_{\mathbf{r},0} , \tag{C3}$$

where we have allowed for possible renormalization of the anisotropy, and introduced $\gamma_l^{-2}\equiv 1-\delta_l$, with

$\gamma_{l=0}^{-2}=\gamma_0^{-2}=(K_\perp/K_\parallel)$. We have defined the derivative operator $\mathbf{D}=(\Delta_\parallel,\gamma_l^{-1}\Delta_z)$, and in Fourier space $U(\mathbf{q})=4\pi[P_\parallel^2+\gamma_0^{-2}P_\perp^2]^{-1}$, with $(\mathbf{P}_\parallel,P_\perp)=(P_x,P_y,P_z)$ and $P_\mu^2\equiv 2-2\cos q_\mu a_\mu$. We first consider the scaling behavior of the $\mathbf{J}\cdot\mathbf{J}$ Hamiltonian term in (C1) and then see how the corrections of βH_1, modify the results, and yield scaling equations for γ_l^{-1}. The argument follows the circular-loop case closely, so we first outline this isotropic model scaling.[17,27]

The partition function can be separated into a part $Z_>$ that involves only loops of scale $>a+da$ and a part δZ that involves interaction of the smallest loops in a range $a,a+da$, with the rest

$$Z=\sum_{\{J^{(L)}\}} e^{-\beta H_>}\prod_L y_l^{(L)}=Z_>+\delta Z\ . \tag{C4}$$

Here $\beta H=\frac{1}{2}\pi K_l\sum_{L\neq L'}\sum_{\mathbf{r},\mathbf{r}'}\mathbf{J}^{(L)}(\mathbf{r})\cdot\mathbf{J}^{(L')}(\mathbf{r}')U(\mathbf{r}-\mathbf{r}')$ involves all the loops of scales $\infty>a_L>a$. $Z_>$ is as in (C4), with a Hamiltonian $\beta H_>$ that involves only loops $a_L>a+da$, while δZ involves the smallest loops $L=1$ in the shell $a,a+da$:

$$\delta Z=\sum_{\substack{\{J^{(L)}\}\\ \text{config}}}\prod_{L(\neq 1)} y_l^{(L)}e^{-\beta H_>}\left[\sum_{\substack{\{J^{(1)}\}\\ \text{config}}} y_l\prod_{L(\neq 1)}\exp\left[-\pi K\sum_{\mathbf{r},\mathbf{r}_1}\mathbf{J}^{(1)}(\mathbf{r}_1)\cdot\mathbf{J}^{(L)}(\mathbf{r})U(\mathbf{r}-\mathbf{r}_1)\right]\right] \tag{C5}$$

with $y_l^{(1)}=y_l$ for the smallest $L=1$ loop. We define the "mirror position" $\mathbf{r}_1^*$ as the position where an oppositely directed segment occurs, $J_\mu^{(1)}(\mathbf{r}_1)=-\mathbf{J}_\mu^{(1)}(\mathbf{r}_1^*)$, so that the small loop acts as a "discrete derivative,"

$$\begin{aligned}\sum_{\mathbf{r}_1}J_\mu^{(1)}(\mathbf{r}_1)U(\mathbf{r}_1-\mathbf{r}')&=\tfrac{1}{2}\sum_{\mathbf{r}_1}J_\mu^{(1)}(\mathbf{r}_1)[U(\mathbf{r}_1-\mathbf{r}')-U(\mathbf{r}_1^*-\mathbf{r})]\\&=\tfrac{1}{2}\sum_{r_1}J_\mu^{(1)}(\mathbf{r}_1)\hat{a}\cdot\Delta_{r_1}U(\mathbf{r}_1-\mathbf{r})\ ,\end{aligned} \tag{C6}$$

where the unit vector $\hat{\mathbf{a}}=[(\mathbf{r}_1-\mathbf{r}_1^*)/a\,]$ spans the loop, and $|\mathbf{r}_1-\mathbf{r}_1^*|=a$ is the circular loop diameter, and the minimum scale.

The term in square brackets in (C5) can then be written, for interaction with two larger-loop segments on loops $L\neq L'$ (i.e., $L,L'\neq 1$),

$$\begin{aligned}[\ ]\simeq\sum_{\{J^{(L)}\}}\sum_{\{J^{(1)}\}} y_l\prod_{\mathbf{r}}^{L}\prod_{\mathbf{r}'}^{L'}&\left[1-\frac{\pi K_l}{2}\sum_{1^{\mathbf{r}}}\mathbf{J}^{(1)}(\mathbf{r}_1)\cdot\mathbf{J}^{(L')}(\mathbf{r})(\hat{a}\cdot\Delta_{\mathbf{r}_1})U(\mathbf{r}_1-\mathbf{r})\right]\\&\times\left[1-\frac{\pi K_l}{2}\sum_{\mathbf{r}_2}\mathbf{J}^{(1)}(\mathbf{r}_2)\cdot\mathbf{J}^{(L')}(\mathbf{r}')(\hat{a}\cdot\Delta_{\mathbf{r}_2})U(\mathbf{r}_2-\mathbf{r}')\right]+\cdots\ .\end{aligned} \tag{C7}$$

By $J_\mu^{(1)}=\pm 1$ symmetry, with a partial integration, shifting the derivative to act on U, and a sum over $J^{(1)}=\pm 1$, the term in square brackets is

$$[\ ]\simeq\sum_{\substack{\{J^{(L)}\}\\ \text{config}}} y_l\left[1-\frac{\pi^2K_l^2}{2}\sum_{\mathbf{r}\neq\mathbf{r}'}\mathbf{J}^{(L)}(\mathbf{r})\cdot\mathbf{J}^{(L')}(\mathbf{r}')\sum_{\mathbf{r}_1}U(\mathbf{r}_1-\mathbf{r})(\hat{\mathbf{a}}\cdot\Delta_{\mathbf{r}_1})^2U(\mathbf{r}_1-\mathbf{r}')\right]\ . \tag{C8}$$

Doing the angular average over the diameter vector $\hat{\mathbf{a}}$ gives $\langle(\hat{\mathbf{a}}\cdot\Delta_{\mathbf{r}_1})^2\rangle U(\mathbf{r}_1-\mathbf{r})=\frac{1}{3}\Delta_{\mathbf{r}_1}^2U(\mathbf{r}_1-\mathbf{r})=-4\pi/3\delta_{\mathbf{r}_1,\mathbf{r}}$. The configuration sum $J^{(1)}$ is over the center of mass $R_{\text{c.m.}}^{(1)}$ and relative $\boldsymbol{\rho}^{(1)}$ coordinates of the $L=1$ loop in a shell $a,a+da$, with the shell integration $\frac{1}{2}a<\rho^{(1)}<\frac{1}{2}(a+da)$ giving $\int d^3\rho^{(1)}/a^3=\frac{1}{2}\pi dl$. The center of mass of the loop $\int d^3R_{\text{c.m.}}^{(1)}/a^3$ gives a volume factor Ω/a^3 for the first terms in the large parentheses of (C7) and allows the delta-function argument in the second, to be satisfied, as R sweeps through the system.

So, finally,

$$\delta Z\simeq\sum_{\substack{\{J^{(L)}\}\\ \text{config}}}\prod_{L\neq 1} y_l^{(L)}e^{-\beta H_>}\left[2\pi y_l dl\frac{\Omega}{a^3}+\frac{2\pi^4}{3}y_l\,dl\,K_l^2\sum\mathbf{J}^{(L)}(\mathbf{r})\cdot\mathbf{J}^{(L')}(\mathbf{r}')U(\mathbf{r}-\mathbf{r}')\right]\ . \tag{C9}$$

Recombining $Z=Z_>+\delta Z$ and reexponentiating, we get a thermal renormalization contribution to coupling,

$$dK_l=-A_0K_l^2y_l dl,\quad A_0\equiv 4\pi^3/3\ , \tag{C10a}$$

and a free-energy density scaling equation $d\beta F_l/a^3=2\pi y_l/a^3dl$.

The loops are now of minimum size $a+da$, but the minimum interloop distance is still a, with potential contributions $\sim\mathbf{J}^{(L)}\cdot\mathbf{J}^{(L')}K_l/a$. Demanding that the minimum loop size is the minimum interloop approach implies an increase in coupling of the $1/R$ potential, $K_l/a=[K_l(1+dl)]/(a+da)$, or an increment

$$dK_l = K_l dl \ . \tag{C10b}$$

This is a geometrical contribution to the coupling K_l that has absorbed a scale a. (For 2D charges q, the potential energy is $\sim q^2 \ln R$, so q^2 is an energy; for 3D q^2 is an energy times a *length*.) Combining the two increments (C11) gives the isotropic case K_l coupling equation (2.7a).

Turning to anisotropic or elliptical loop scaling, the argument carries through largely as before, but with four differences: (i) The $\mathbf{r}_1 - \mathbf{r}_1^*$ vector across the ellipse is not a constant, as it rotates through the ellipse perimeter, and the equation obeyed by U is (C3); (ii) the shell volume in the scale $a, a+da$ is around an elliptical, not circular perimeter, (iii) U is explicitly dependent on the scale-dependent anisotropy γ_l^{-1}, and (iv) the fugacity $y_l(\alpha)$ depends on the angle α between the z axis and the ellipse minor axis, which could weight angular averages previously done freely over tumbling smaller loops. Angular averages $\langle\ \rangle$ include an average over α with weight $y_l(\alpha)/\bar{y}_l$, where $\bar{y}_l$ is the free angular average of $y_l(\alpha)$.

The corresponding modifications of the argument are as follows.

(i) Defining $\mathbf{R} \equiv [(\mathbf{r}-\mathbf{r}^*)_\parallel, \gamma_l(\mathbf{r}-\mathbf{r}^*)_\perp]$, the ellipse is given by (2.19), i.e., $\mathbf{R}^2 = a^2$. Then, from (C3), the angular average over all segments and over all loop orientations,

$$\langle [(\mathbf{r}_1 - \mathbf{r}_1^*)/a)\cdot\boldsymbol{\Delta}]^2 \rangle U = \langle [(\mathbf{R}/a)\cdot\mathbf{D}]^2 \rangle U$$
$$\approx \tfrac{1}{3}\mathbf{D}^2 U = -\frac{4\pi}{3}\delta_{\mathbf{r},0} \tag{C11}$$

[where (iv) below has been anticipated in the approximate equality].

(ii) The dl factor from the $a, a+da$ shell in the configuration integral is changed by the ratio of the elliptical to the circular perimeter. From (2.19) and (1.9)

$$\pi\, dl \to \pi\, dl \left[\int_0^{2\pi} d\phi (x^2+\eta^2)^{1/2}/\pi a \right]$$
$$= \pi\, dl \int_0^{\pi/2} \frac{d\phi}{\pi/2} (1 - e^2 \sin^2\phi)^{1/2}$$
$$\approx \pi\, dl [1 - \tfrac{1}{2}\langle e^2(\alpha)\rangle] \ , \tag{C12}$$

where $e = e(\alpha)$ is the eccentricity. For $\delta_l \equiv 1 - \gamma_l^{-2} \ll 1$, anticipating the result that $\gamma_l^{-1} \to 1$ asymptotically, the net change is

$$\pi\, dl \to \pi\, dl [1 - \tfrac{1}{4}\delta_l] \ . \tag{C13}$$

(iii) The scale dependence of the effective anisotropy γ_l^{-1} in U generates a new additional potential

$$\frac{|\mathbf{J}(\mathbf{q})|^2}{\mathbf{P}_\parallel^2 + \gamma_l^{-2} P_z^2} \approx \frac{|\mathbf{J}(\mathbf{q})|^2}{\mathbf{P}_\parallel^2 + \gamma_{l+dl}^{-2} P_z^2}$$
$$- \frac{[(d\delta_l/dl)dl P_z^2]|\mathbf{J}(\mathbf{q})|^2}{(\mathbf{P}_\parallel^2 + \gamma_l^{-2} P_z^2)^2} \ . \tag{C14}$$

The additional term is asymptotically small, with coefficient shown below scaling to zero, and so it is dropped.

(iv) The angular average of $y_l(\alpha)$ and other α-dependent scaling factors, such as above, can be approximated by the product of the free angular averages, with corrections that are higher order in $\delta_l y_l$. Thus, the angularly averaged fugacity $\bar{y}_l$ just replaces the previous, isotropic fugacity. Thus the K_l scaling equation is to $O(\delta_l \bar{y}_l)$,

$$\frac{dK_l}{dl} \approx K_l - A_0 K_l^2 \bar{y}_l \tag{C15}$$

as in (3.2a).

Other explicit scale dependences are absorbed in the fugacity. The unit-cell a^3 scale factors in the configuration integrals [center-of-mass and relative coordinates $(\int d^3 R_{\text{c.m.}}^{(L)}/a^3)(\int d^3\rho^{(L)}/a^3)$ for each loop L] give a renormalization increment $d\bar{y}_l = 6 dl \bar{y}_l$. The explicit scale dependence of the fugacity (2.21) and of the anisotropy γ_l^{-1} give collecting contributions,

$$d\bar{y}_l \approx 6\bar{y}_l dl - \pi^2 K_l L_l \bar{y}_l dl + \tfrac{1}{2}\beta E_0(a)\delta_l \langle \sin^2\alpha \rangle \bar{y}_l dl \ , \tag{C16}$$

with $L_l \equiv 1 + \ln(a/a_c)$, an angular average $\langle\ \rangle$ over α with weight $y_l(\alpha)/\bar{y}_l$. Thus, to relative order δ_l, shown later to scale to zero,

$$\frac{dy_l}{dl} \approx (6 - \pi^2 K_l L_l)\bar{y}_l \ . \tag{C17}$$

We now consider the scaling of the rotationally noninvariant βH_1 of (C2), and obtain the scaling equation for γ_l^{-1}. Including both direct terms from $\beta H_1 \beta H_1$ in (C2) and the cross term $\beta H_0 \beta H_1$ in (C1), the scaling of the coefficient, of the $+\mathbf{J}\cdot\mathbf{J}$ term of $C(2)$, to $O(\delta_l)$, goes as

$$\frac{d(1-\gamma_l^{-1})}{dl} = -A_0 K_l \bar{y}_l (1 - \gamma_l^{-1}) \ . \tag{C18}$$

In obtaining (C18), we must go through arguments such as (C7) and (C8) for the isotropic case and use relations as given below in an obvious notation (suppressing arguments for simplicity). Using (C11)

$$4\sum \mathbf{J}\cdot\mathbf{J}U\mathbf{J}\cdot\mathbf{J}U = -\sum\sum_\mu J_\mu J_\mu U(\hat{a}_\mu \Delta_\mu)^2 U$$
$$= -\sum \mathbf{J}\cdot\mathbf{J}U\tfrac{1}{3}\mathbf{D}^2 U = \frac{4\pi}{3}\sum \mathbf{J}\cdot\mathbf{J}U \ ,$$
$$4\sum J\otimes JUJ\otimes JU = -\sum\sum_\mu J_\mu J_\mu A_{\mu\mu}^2 U(\hat{a}_\mu\Delta_\mu)^2 U$$
$$= -\sum JJU\tfrac{1}{3}\mathbf{D}^2 U = \frac{4\pi}{3}\sum \mathbf{J}\cdot\mathbf{J}U \ , \tag{C19}$$
$$4\sum J\otimes JU\mathbf{J}\cdot\mathbf{J}U = -\sum\sum_\mu J_\mu J_\nu U A_{\mu\nu}(\hat{a}_\mu\Delta_\mu)^2 U$$
$$= -\sum J\otimes J\tfrac{1}{3}\mathbf{D}^2 U = \frac{4\pi}{3}\sum J\otimes JU \ ,$$

The common fixed point of (C18) and (C15) is clearly the 3D fixed point unchanged, $A_0 K^* y^* = 1$ and $1 - (\gamma^{-1})^* = 0$. In the vicinity, to $O(\delta_l^2)$, (C18) gives

$$\delta_l \equiv 1 - \gamma_l^{-2} \approx (1 - \gamma_0^{-2}) e^{-l} \ . \tag{C20}$$

The coefficient g_l can be shown from (C20) to be well behaved, not changing these conclusions. Near the fixed point, with relative order corrections $\sim\delta_l^2$, $(1-A_0K_ly_l)g_l$ is dropped, so

$$\frac{dg_l}{dl}\sim -2A_0K_ly_l\approx -2\ , \tag{C21}$$

i.e., $g_l\sim g_0-2l$. Thus, since $(1-\gamma_l^{-1})\sim e^{-l}\to 0$, the βH_1 contribution of (C2) scales to zero, and the $\mathbf{J}\cdot\mathbf{J}$ first Hamiltonian term of (C1) determines the $K_l,\bar{y}_l$ scaling equations.

Note that in the strongly anisotropic regime $\gamma_0^{-2}<0.25$ the quasi-2D *HT* excitations, which scale as (4.13), dominate for scales $a<r_0$. The 3D scaling equations and renormalization of γ_l^{-1} cut in only for $l>l_0$, so (C20) is replaced, for $\gamma_0^{-1}<0.5$, by

$$1-\gamma_l^{-1}\approx(1-\gamma_0^{-1})e^{-(l-l_0)}\ . \tag{C22}$$

[1]G. Burns, *High Temperature Superconductivity* (Academic, New York, 1992).

[2]W. A Little, Science **242**, 1390 (1988).

[3]P. Chaudhuri *et al.*, IBM J. Res. Dev. **33**, 299 (1989).

[4]M. N. Keene, T. J. Jackson, and C. E. Gough, Nature (London) **340**, 210 (1989).

[5]S. Martin, A. T. Fiory, R. M. Fleming, G. P. Espinoa, and S. A. Cooper, Phys. Rev. Lett. **62**, 677 (1989).

[6]S. Vadlamannati, Q. Li, T. Venkatesan, W. L. McLean, and P. Lindenfeld, Phys. Rev. B **44**, 7094 (1991).

[7]J. M. Kosterlitz and D. J. Thouless, J. Phys. C **6**, 1181 (1973); V. Berezinskii, Zh. Eskp. Teor. Fiz. **61**, 1144 (1971) [Sov. Phys. JETP **34**, 610 (1971)].

[8]C. J. Lobb, Physica B+C **152**, 319 (1988).

[9]J. M. Kosterlitz, J. Phys. C **7**, 1046 (1974).

[10](a) H. Jensen and P. Minnhagen, Phys. Rev. Lett. **66**, 1630 (1991); (b) V. Cataudella and P. Minnhagen, Physica, C **166**, 442 (1990); (c) H. Weber and H. J. Jensen, Phys. Rev. B **44**, 454 (1991); (d) P. Minnhagen, Helv. Phys. Act. **65**, 205 (1992); (e) P. Minnhagen and P. Olsson, Phys. Rev. B **44**, 4503 (1991); Phys. Rev. Lett. **67**, 1039 (1991); Phys. Rev. B **45**, 5722 (1992); M. Friesen, Phys. Rev. B **51**, 632 (1995); (f) S. Pierson, Phys. Rev. Lett. **73**, 2496 (1994).

[11](a) S. Korshunov, Europhys. Lett. **11**, 757 (1990); (b) L. N. Bulaevskii, M. Ledvij and V. G. Kogan, Phys. Rev. Lett. **68**, 3773 (1992); (c) B. Horowitz, Phys. Rev. B **45**, 12 631 (1992); (d) S. N. Artemenko, I. G. Gorlova, and Yu. I. Latyshev, Phys. Lett. A **138**, 428 (1989); (e) S. W. Pierson and O. T. Valls, Phys. Rev. B **45**, 13 076 (1992); (f) K. H. Fischer, Physica C **210**, 179 (1993).

[12]M. B. Salamon, J. Shi, N. Orevend, and M. A. Howson, Phys. Rev. B **43**, 5520 (1993); T. Schneider and D. Ariosa, Z. Phys. B **89**, 267 (1992); S. Kamal *et al.*, Phys. Rev. Lett. **73**, 1845 (1994).

[13]J. Friedel, J. Phys. (Paris) **49**, 1561 (1988); **49**, 1769 (1988).

[14]P. C. E. Stamp, L. Forro, and C. Ayache, Phys. Rev. B **38**, 2847 (1988); P. C. E. Stamp, Phys. Rev. Lett. **63**, 582 (1989); S. Martin, A. T. Riory, R. M. Fleming, G. P. Ariosa, and A. S. Cooper, *ibid.* **63**, 583 (1989).

[15]D. Ariosa and H. Beck, Phys. Rev. B **43**, 344 (1991); D. Schmeltzer and A. R. Bishop, *ibid.* **41**, 9603 (1990).

[16]G. A. Williams, Phys. Rev. Lett. **59**, 1926 (1987); Physica **165**, 769 (1990); Phys. Rev. Lett. **68**, 2054 (1992); J. Low Temp. Phys. **89**, 91 (1992); Phys. Rev. Lett. **71**, 392 (1993).

[17](a) S. R. Shenoy, Phys. Rev. B **40**, 5056 (1989); (b) Phys. Rev. B **42**, 8595 (1990); (c) Helv. Phys. Acta. **65**, 477 (1992); (d) Current Sci. (Bangalore) **65**, 392 (1993). Copies available on request.

[18](a) T. Banks, R. Myerson, and J. Kogut, Nucl. Phys. **B129**, 493 (1977); (b) R. Savit, Phys. Rev. B **17**, 1340 (1978); Rev. Mod. Phys. **52**, 453 (1980).

[19]S. R. Shenoy, Phys. Rev. Lett. **72**, 400 (1994); and (unpublished).

[20]C. Dasgupta and B. Halperin, Phys. Rev. Lett. **21**, 1556 (1981).

[21]R. A. Klemm, A. Lutter, and M. R. Beasley, Phys. Rev. B **12**, 877 (1975), and references therein.

[22]R. P. Feynman, Prog. Low. Temp. Phys. **1**, 36 (1955); L. Onsager, Nuovo Cimento **6**, Suppl. 2, 249 (1949); E. Byckling, Ann. Phys. (N.Y.) **32**, 367 (1965).

[23]B. I. Halperin, in *Physics of Defects,* Proceedings of the Les Houches Session XXXV, 1980, edited by R. Balian, M. Kleman, and J. P. Pourier (North-Holland, New York, 1981).

[24](a) C. Kawabata and K. Binder, Ann. Israel Phys. Soc. **2**, 988 (1978); (b) H. Kleinert, *Gauge Fields in Condensed Matter Physics* (World Scientific, Singapore, 1989), Vol. 1; (c) W. Janke and T. Matsui, Phys. Rev. B **42**, 10 673 (1990); (d) A. Schmidt and T. Schneider, Z. Phys. B **87**, 265 (1992).

[25](a) J. Epiney, diploma thesis, ETH Zurich, 1990; J. Epiney and Ph. De Forcrand (unpublished); (b) D. Baeriswyl, X. Bagnoud, A. Chiolero, and M. Zamora, Brazilian J. Phys. **22**, 140 (1992); (c) S. T. Chui and Giri, Phys. Lett. A **128**, 49 (1988).

[26]G. Kohring, R. Shrock, and P. Wills, Phys. Rev. Lett. **61**, 2970 (1987).

[27]B. Chattopadhyay, M. C. Mahato, and S. R. Shenoy, Phys. Rev. B **47**, 15 159 (1992).

[28]S. Hikami and T. Tsuneto, Prog. Theor. Phys. **63**, 387 (1980).

[29]J. Gilliou and J. Zinn-Justin, Phys. Rev. B **21**, 3976 (1989).

[30]N. Gupte and S. R. Shenoy, Phys. Rev. B **31**, 3150 (1985).

[31]Deviations of the theoretical curve from the MC data [Refs. 25(a) and 25(b)] are apparent in Fig. 5(a), e.g., for $\gamma_0^{-2}>8$. The major axis for $\gamma_0^{-1}>1$ is $\sim a\gamma_0^{-1}$ for a tumbling loop at $\alpha=0$ orientation, and we must have, in a simulation $a\gamma_0^{-1}\ll L$, the system size. For $L\sim 16a_0$, loops of $\frac{1}{3}$ the system size would be constrained, and T_c probably raised, for $\gamma_0^{-2}>8$.

[32]T. Ohta and D. Jasnow, Phys. Rev. B **20**, 139 (1979).

[33]In experiments (Ref. 5) $T_{\rm KT}$ is treated as a fitted parameter to optimize the 2D behavior. Here we take $T_{\rm KT}$ as almost fixed by the $\pi K_{l_0}(\bar{T}_{\rm KT})=2$ criterion, but in plots, it is varied by about 2% around this value to optimize linearity.

[34]R. Fazio and G. Schön, Phys. Rev. B **43**, 5507 (1991).

[35]H. M. Jaeger, D. B. Haviland, A. M. Goldman, and B. G. Orr, Phys. Rev. B **34**, 4920 (1986).

[36]W. Janke and H. Kleinert, Nucl. Phys. B **270**, 135 (1986).

[37](a) I. S. Gradhshteyn and I. M. Ryzhik, *Tables of Integrals, Series and Products* (Academic, New York, 1965), pp. 152 and 262, and (b) p. 905.